REPORT SD-TR-89-45

Photolysis of Spacecraft Contaminants

T. B. STEWART, G. S. ARNOLD, D. F. HALL, and H. D. MARTEN
Chemistry and Physics Laboratory
Laboratory Operations
The Aerospace Corporation
El Segundo, CA 90245

1 July 1989

Prepared for

SPACE SYSTEMS DIVISION
AIR FORCE SYSTEMS COMMAND
Los Angeles Air Force Base
P.O. Box 92960
Los Angeles, CA 90009-2960

UNCLASSIFIED

SECURITY CLASSIFICATION OF THIS PAGE

REPORT DOCUMENTATION PAGE

1a. REPORT SECURITY CLASSIFICATION Unclassified	1b. RESTRICTIVE MARKINGS
2a. SECURITY CLASSIFICATION AUTHORITY	3. DISTRIBUTION/AVAILABILITY OF REPORT Approved for public release; distribution unlimited.
2b. DECLASSIFICATION/DOWNGRADING SCHEDULE	
4. PERFORMING ORGANIZATION REPORT NUMBER(S) TR-0086(6403-01)-1	5. MONITORING ORGANIZATION REPORT NUMBER(S) SD-TR-89-45
6a. NAME OF PERFORMING ORGANIZATION The Aerospace Corporation Laboratory Operations 6b. OFFICE SYMBOL *(If applicable)*	7a. NAME OF MONITORING ORGANIZATION Space Systems Division
6c. ADDRESS *(City, State, and ZIP Code)* El Segundo, CA 90245	7b. ADDRESS *(City, State, and ZIP Code)* Los Angeles Air Force Base Los Angeles, CA 90009-2960
8a. NAME OF FUNDING/SPONSORING ORGANIZATION 8b. OFFICE SYMBOL *(If applicable)*	9. PROCUREMENT INSTRUMENT IDENTIFICATION NUMBER F04701-85-C-0086
8c. ADDRESS *(City, State, and ZIP Code)*	10. SOURCE OF FUNDING NUMBERS PROGRAM ELEMENT NO / PROJECT NO / TASK NO / WORK UNIT ACCESSION NO.

11. TITLE *(Include Security Classification)*
PHOTOLYSIS OF SPACECRAFT CONTAMINANTS

12. PERSONAL AUTHOR(S)
Stewart, Thomas B.; Arnold, Graham S.; Hall, David F.; Marten, H. Daniel

13a. TYPE OF REPORT	13b. TIME COVERED	14. DATE OF REPORT *(Year, Month, Day)*	15. PAGE COUNT
	FROM _____ TO _____	1 July 1989	68

16. SUPPLEMENTARY NOTATION

17. COSATI CODES			18. SUBJECT TERMS *(Continue on reverse if necessary and identify by block number)*		
FIELD	GROUP	SUB-GROUP	contamination	siloxane	radiator
			photochemistry	phthalate	
			photodeposition	solar absorptance	

19. ABSTRACT *(Continue on reverse if necessary and identify by block number)*

Self-contamination of sensitive spacecraft surfaces has long been recognized as potentially limiting the performance, and even the useful life, of a spacecraft. It has become clear that photochemical reactions, induced by solar vacuum ultraviolet (VUV) illumination, play a substantial role in contaminant deposition. A series of laboratory measurements of the absolute rates of adsorption, desorption, and VUV-induced deposition of contaminants under simulated spacecraft conditions are described in this report. The rates measured are sufficient to explain anomalous radiator degradation on the Satellite Data Systems spacecraft radiator. The dependence of the deposition rate on substrate identity and temperature and on contaminant identity and flux is discussed, and a simple kinetic model that describes most experimental observations is presented.

20. DISTRIBUTION/AVAILABILITY OF ABSTRACT	21. ABSTRACT SECURITY CLASSIFICATION	
☐ UNCLASSIFIED/UNLIMITED ☒ SAME AS RPT. ☐ DTIC USERS	Unclassified	
22a. NAME OF RESPONSIBLE INDIVIDUAL	22b. TELEPHONE *(Include Area Code)*	22c. OFFICE SYMBOL

DD FORM 1473, 84 MAR 83 APR edition may be used until exhausted. All other editions are obsolete

SECURITY CLASSIFICATION OF THIS PAGE
UNCLASSIFIED

PREFACE

It is a pleasure to acknowledge the contributions of J. H. Hecht, L. J. Ortega, and E. R. Schnauss in the initiation of the experimental program and of A. R. Calloway in the design and fabrication of the vacuum ultraviolet resonance lamps. The authors further express their gratitude to R. R. Hayes and E. A. Zeiner for many useful discussions during the course of this work and to H. K. A. Kan for technical guidance.

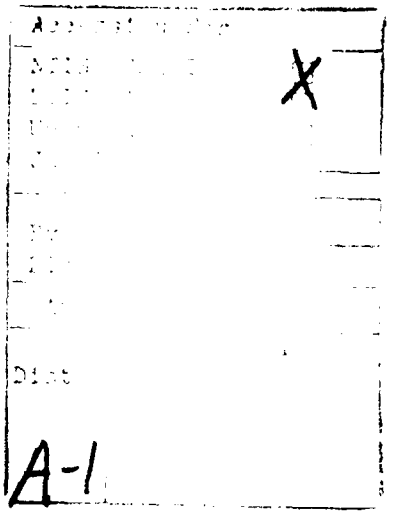

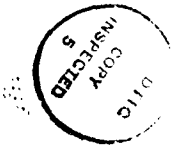

CONTENTS

FIGURES

FIGURES (Continued)

TABLES

I. INTRODUCTION AND EXECUTIVE SUMMARY

As the complexity, expense, and size of spacecraft increase, the need to understand and predict the effects of the space environment (both ambient and induced) on spacecraft performance increases. Such an understanding is necessary to permit spacecraft hardware and operations to be designed to guarantee sufficient useful lifetime of the system. In addition to the deleterious effects of the space radiation, charged particle, and neutral environments, self-contamination of spacecraft surfaces has long been recognized as potentially limiting the performance, and even the useful life, of a spacecraft.

Among the most contamination-sensitive areas of any spacecraft are the heat radiators, which are often mosaics of fused silica second-surface mirrors. Accretion of contaminant films on a radiator increases its solar absorptance (alpha), thereby causing a temperature rise in the whole vehicle. Figure 1 indicates the wide variation in the alpha degradation rate exhibited by satellite radiators.[1] Differences in the radiation environments of the various vehicles' orbits may account for some of this variation; however, the dominant factor is most likely the variation in the contaminant accretion rate.

In the past it was considered that cold surfaces, or at least surfaces at temperatures below those of the contaminant molecule sources, were most likely to accumulate contaminant layers. The observation of a high alpha degradation rate on the Satellite Data System (SDS) vehicle's radiator was surprising because the radiator was sunlit, causing it to be warmer than most potential sources of contamination. The best theory of this unexpected warming is that sunlight causes photochemical deposition of contaminants on fused silica, thereby increasing the radiator solar absorptance.

Evidence for such a deposition process was obtained from the United States Air Force (USAF) Space Test Program vehicle P78-2, commonly known as

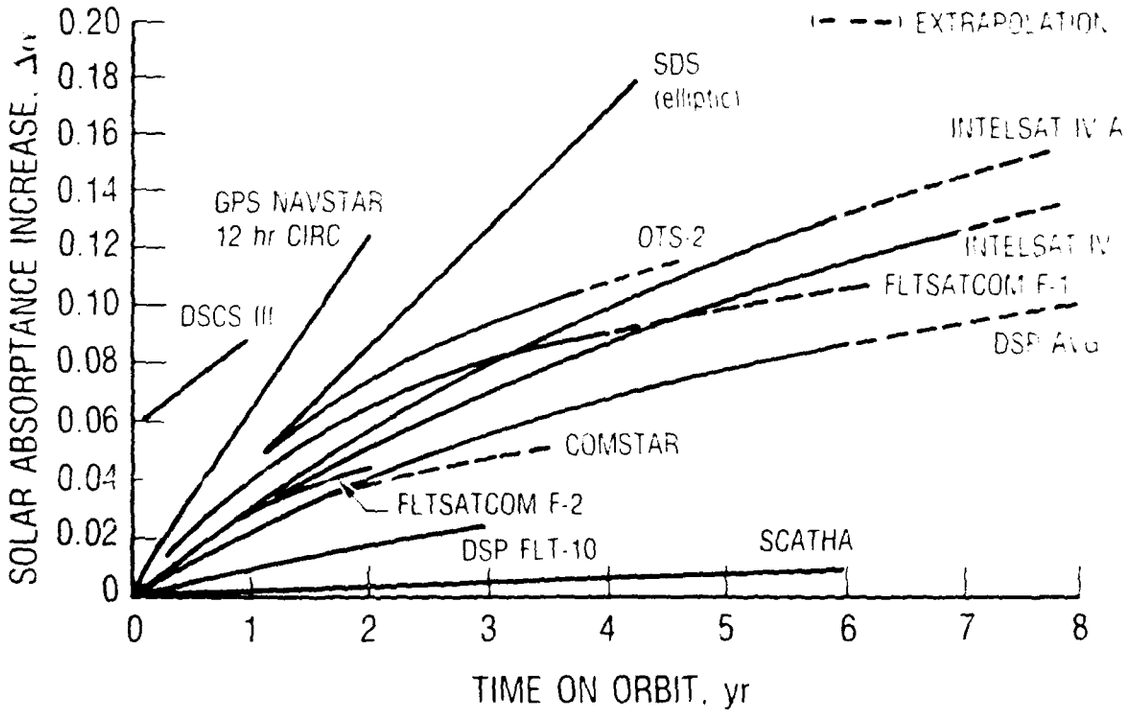

Fig. 1. Increase in the Solar Absorptance Property of Silvered Fused Silica Mirror Radiators for Several Satellites

the Spacecraft Charging at High Altitudes (SCATHA) spacecraft.[2] One experiment on the spacecraft included a pair of temperature-controlled quartz crystal microbalances (TQCMs) that measured the temperature-dependent rate of contaminant accretion on the spacecraft's surface. The SCATHA vehicle is a spin-stabilized (at a nominal attitude of 90 deg) satellite in an approximately geostationary orbit. One of the TQCMs was located on the spinning "bellyband" of the spacecraft; the other was on the top platform. The bellyband TQCM is sunlit for a portion of the satellite revolution. The top TQCM is always shadowed. The shadowed TQCM has a portion of the main satellite antenna in direct line of sight. The sunlit sensor has only a small view of some experimental hardware, at a great distance. Thus one might expect the shadowed sensor to experience more direct flux of outgassed contaminants.

Figure 2 indicates that the sunlit sensor accumulates mass at a substantially higher rate than the shadowed sensor.[1] Figure 3 indicates the temperature history and the mass accretion history of the sunlit sensor.[3] The mass accumulation rate on the sunlit surface does not strongly depend on the temperature of the TQCM. In fact, deposition has been observed on this surface at temperatures that were in excess of the contaminant source's temperature on the spacecraft. Conversely, the mass accumulation rate for the shadowed sensor is quite strongly dependent upon the substrate temperature (see, for example, Table 1 of Ref. 2). These observations, summarized in Figs. 2 and 3, suggest that solar vacuum ultraviolet (VUV) radiation accelerates the rate of contaminant deposition on surfaces of the SCATHA satellite and that an irradiated contaminant has a greater tenacity than a contaminant deposited on the shadowed sensor.

Additional evidence supporting the hypothesis that UV radiation is responsible for the accretion of contaminants on spacecraft surfaces was obtained from two separate laboratory experiments. In one experiment,[4] Kruger and Shapiro at the National Aeronautics and Space Administration/ Goddard Space Flight Center (NASA/GSFC), using a mercury "pen-ray" lamp in a "dirty" vacuum system, detected mass deposition on a TQCM exposed to this

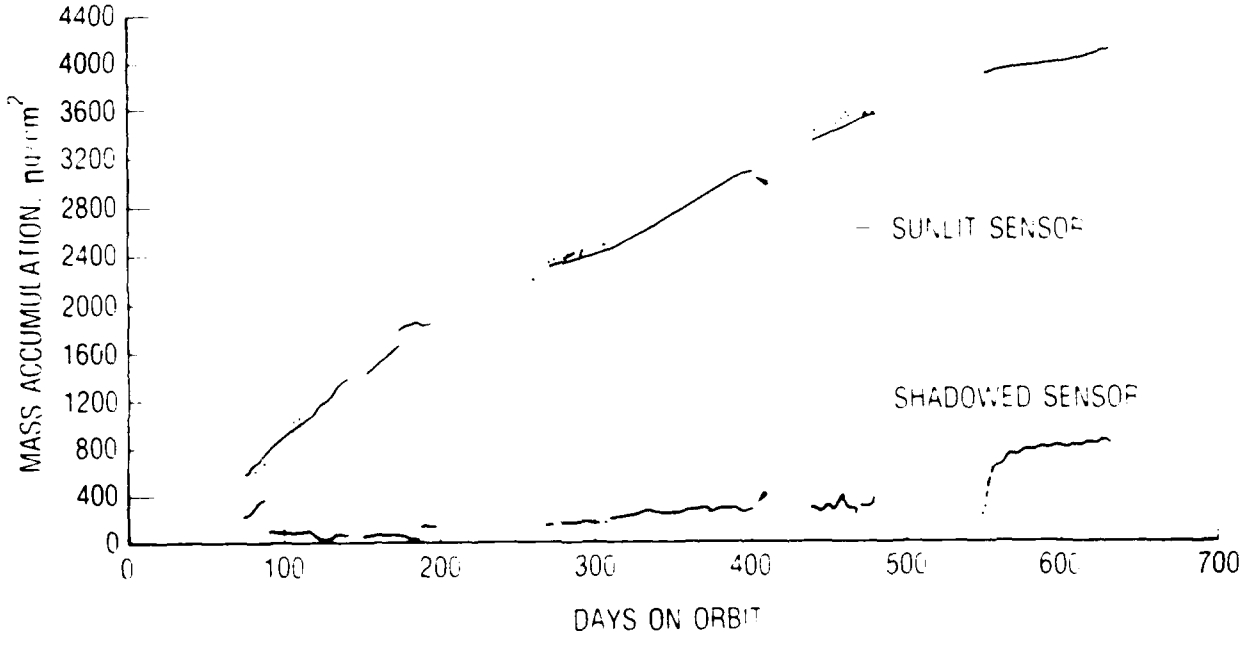

Fig. 2. Mass Accumulation on the SCATHA ML-12 Temperature Controlled Quartz Crystal Microbalances

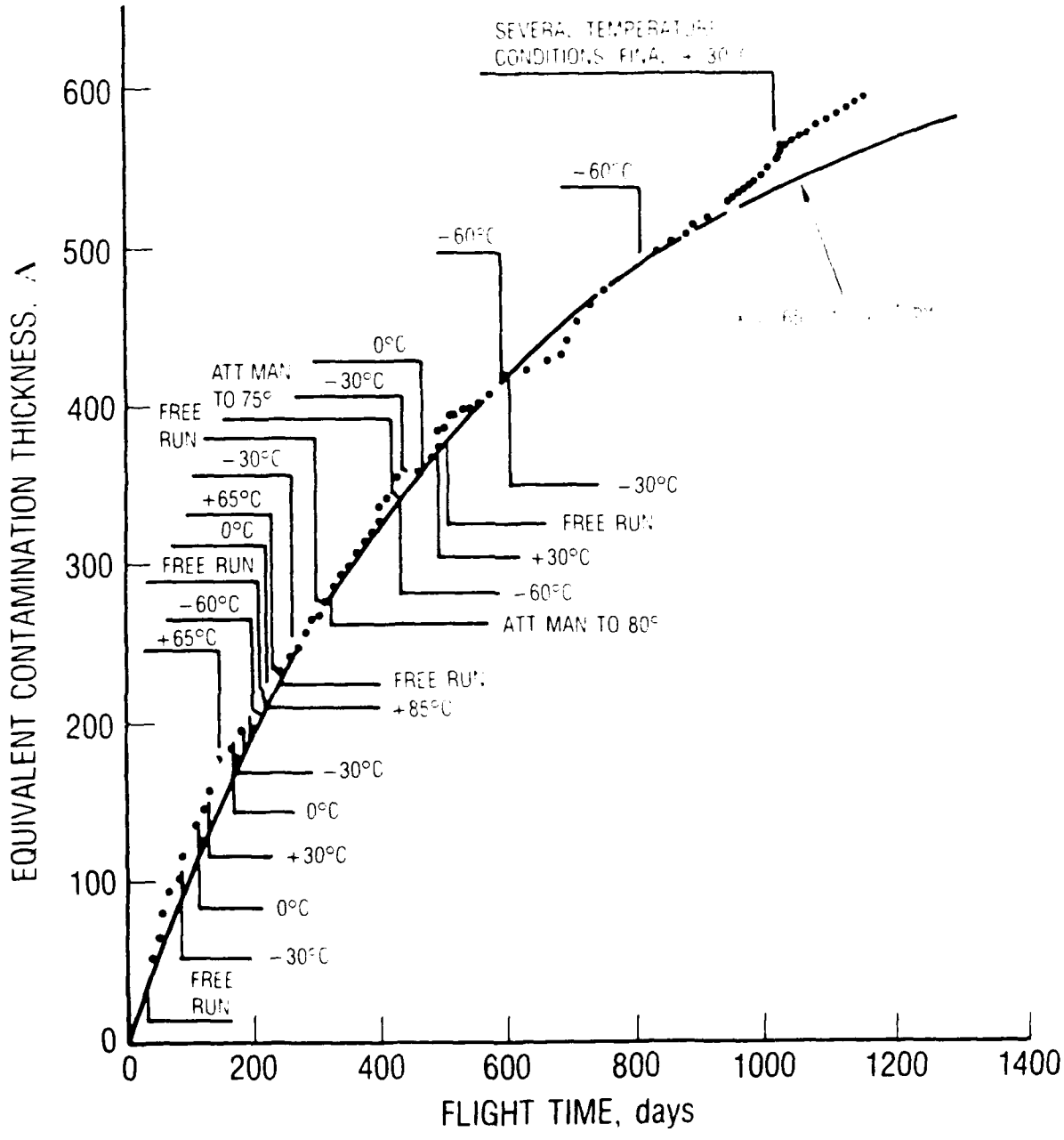

Fig. 3. Time and Temperature History of the Mass Accumulation Rate on the Sunlit SCATHA ML-12 Temperature Controlled Quartz Crystal Microbalance

UV radiation. They did not detect any mass accumulation on a companion TQCM shielded from UV radiation by a Pyrex filter. The second experiment conducted by Hayes at Hughes Aircraft, under more controlled conditions, observed the UV-enhanced photodeposition of volatile materials outgassed from RTV-511 solar cell adhesive and other materials.[1]

These laboratory results, along with the SCATHA ML-12 results, suggested the feasibility of photochemical deposition as the cause of SDS radiator degradation. However, there was insufficient quantitative rate data available to draw this conclusion unambiguously. It was estimated that the SDS radiator surface experienced a total molecular flux of less than 0.4 $\mu g\ cm^{-2}\ h^{-1}$ (which would correspond to a molecular arrival rate of 40 $Å\ h^{-1}$, if all the incident flux were to deposit into a film of 1 $g\ cm^{-3}$ density), and the relative temperature of the sources and collectors were such that condensation was not expected to occur. A deposition rate of approximately 1 $ng\ cm^{-2}\ h^{-1}$ (0.1 $Å\ h^{-1}$) was necessary to explain the rate of increase in solar absorption of the vehicle radiator.

The initial investigations by Hayes[1] were performed with fluxes of molecules (outgassing from spacecraft engineering materials) much higher than this expected value. If one extrapolated Hayes's results linearly to the appropriate molecular arrival rates, then one would conclude that it was unlikely that photochemical deposition could proceed at a rate necessary to explain the observed radiator degradation. However, Hayes's background photochemical deposition rate (resulting from chamber residual gas) suggested that a linear extrapolation was inappropriate.

The work discussed in this report extended the measurement of absolute deposition rates into the regime of molecular arrival rates expected on orbit. Figure 4 is a compilation of the laboratory measured deposition rates of model contaminants DC-704 and diethylhexylphthalate [dioctylphthalate (DEHP)], for a variety of substrate conditions, in addition to the results of Hayes. From this figure, one can readily discern the nonlinear dependence of the deposition rate on the molecular arrival rate.

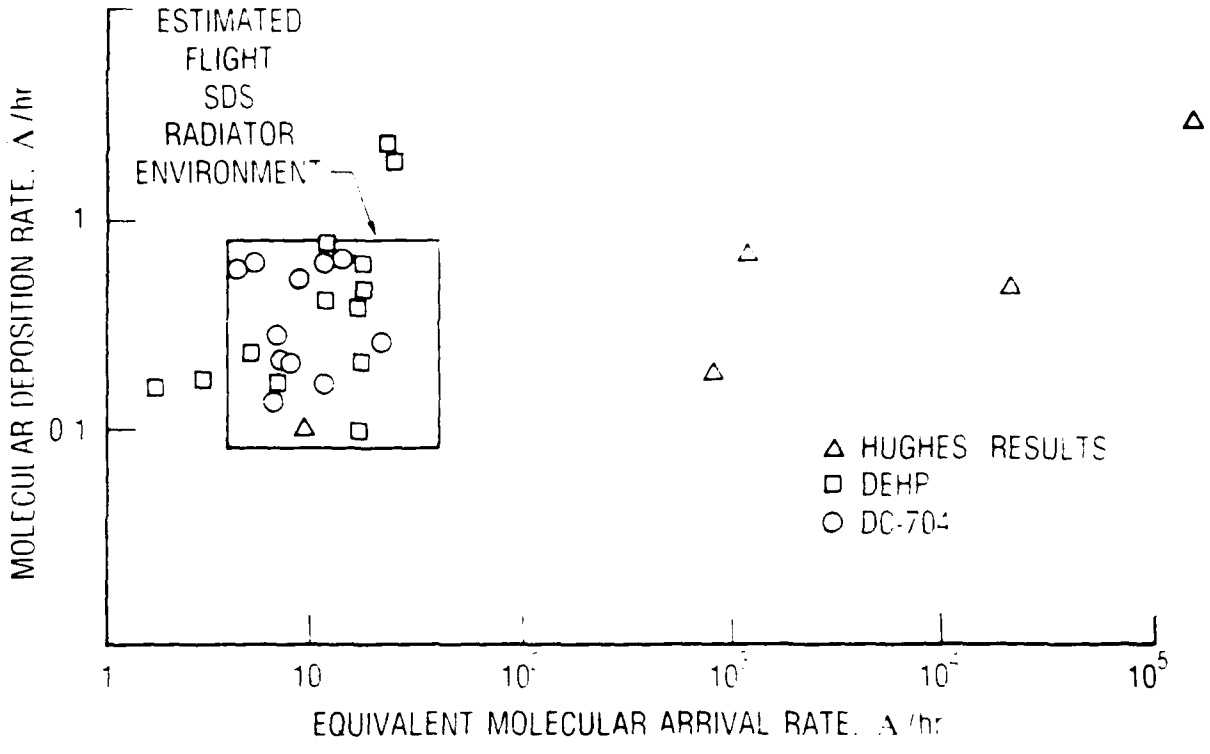

Fig. 4. Compilation of Photochemical Deposition Rates versus Arrival Rate for DC-704 and DEHP for a Variety of Substrate Compositions and Temperatures. Also shown are results from Hughes Aircraft Company experiments (see Ref. 1).

The box in Fig. 4 represents the range of predicted molecular arrival rates and deposition rates necessary to explain the observed increase in solar absorptance of the SDS satellite radiator.[1] The deposition rates measured in this work fall within the predicted range for a realistic range of substrate temperatures, for two molecules typical of spacecraft outgassing contaminants. Therefore, these results indicate that the unexpected increase in solar absorptance on the SDS radiator can be ascribed to photochemical contaminant deposition. These results and data from the SCATHA ML-12[3] spaceflight experiment show quantitatively that solar UV irradiation does not merely darken or fix previously condensed contaminant films.[5,6] Solar UV irradiation can also affect the rate at which those films accrete, similar to photopolymerization reactions observed in other laboratory experiments.[7,8]

Section II of this report describes the experimental apparatus and procedures used in this work. Section III presents the results of measurements of absolute rates of adsorption, desorption, and photochemical deposition of two large organic molecules that are representative of the sorts of contaminants that outgas from nonmetallic spacecraft construction materials.

These results, and the discussion that follows in Section IV of this report, show that the photochemical deposition of contaminant films under the conditions that prevail on sunlit spacecraft surfaces is a competition between photolysis and desorption of a transiently adsorbed contaminant precursor molecule. A simple kinetic model in the spirit of the Langmuir model[9] of adsorption on surfaces is presented in Section IV. Using experimentally measured parameters, this model is reasonably successful in describing the deposition process.

II. EXPERIMENTAL

This section briefly describes the apparatus used to measure absolute rates of photochemical deposition of organic films under conditions expected to prevail on sunlit spacecraft surfaces. Procedures are described that were used to measure the residence time of a potential contaminant molecule on a surface (in the absence of illumination), the number of molecules per unit area that make up a contaminant monolayer, and the rate of (irreversible) photochemical contaminant deposition.

A. APPARATUS

These experiments were performed in an ultrahigh vacuum system evacuated with a turbomolecular pump and a liquid nitrogen cooled (110 K) shroud to pressures of about 2×10^{-9} Torr. Thus possible interference from background contaminants in the chamber was greatly reduced.

Figure 5 is a schematic representation of the experimental apparatus. The major elements of this apparatus are a temperature-controlled quartz crystal microbalance (TQCM) for mass detection, a Knudsen cell or effusive molecular beam source of organic molecules, interchangeable vacuum ultraviolet (VUV) lamps, and a shutter for switching the molecular beam on and off to the TQCM.

One major difference between the experiments described in this report and some other spacecraft contamination experiments is the use of model contaminant molecules. Rather than using the outgassing products of engineering materials as the contaminant flux, molecular beams of pure materials that represent the kinds of molecules that outgas from spacecraft materials were used. This made it possible to direct controlled, constant fluxes of potential contaminant molecules at the test surface. Two different model compounds were used: a siloxane (DC-704) and an aromatic ester (DEHP). The details of TQCM signal averaging, Knudsen cell calibration, VUV lamp construction and calibration, and deposition witness samples are discussed more completely in Appendix A.

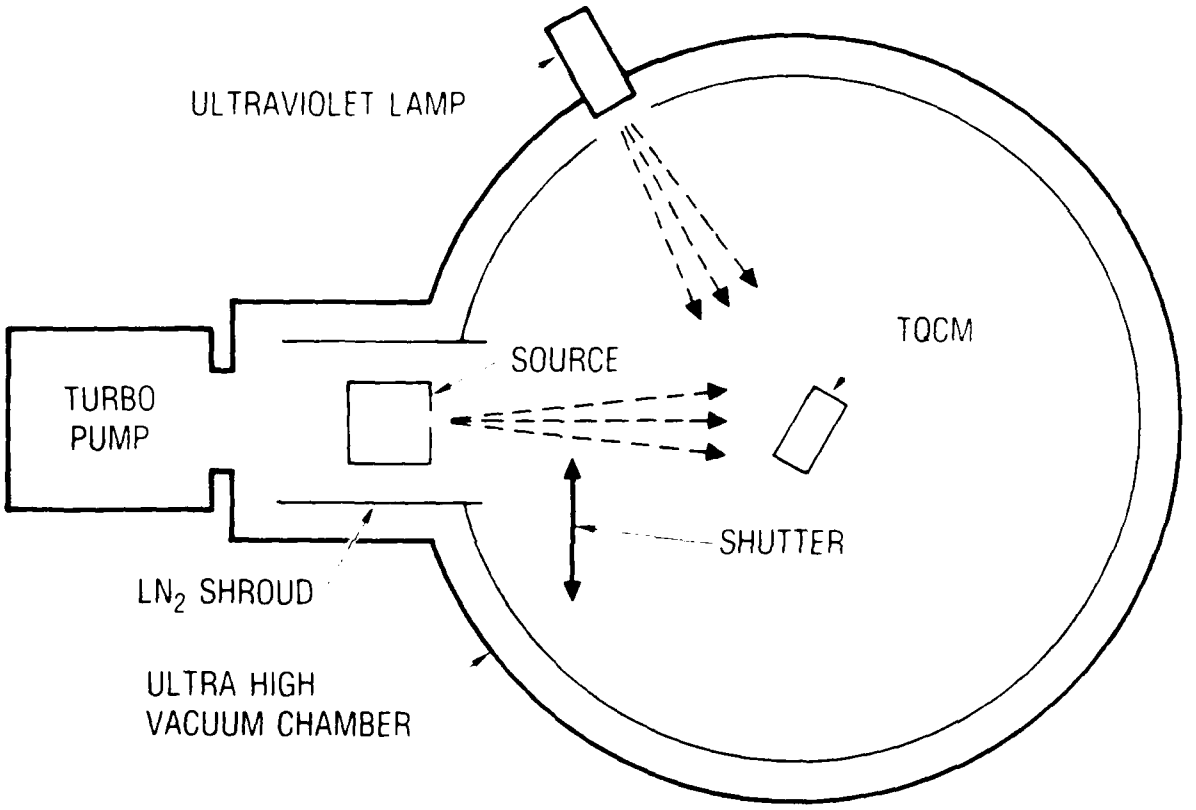

Fig. 5. Schematic Representation of the Photochemical Deposition Apparatus

B. EXPERIMENTAL PROCEDURES

These experiments were undertaken upon the hypothesis that photochemical deposition is a competition between photolysis and desorption of a transiently adsorbed molecule. (The algebra of this model is presented in Appendix B.) Such a picture suggests the utility of measuring not only photochemical deposition rates, but also thermal desorption rate coefficients and effective surface site densities (via adsorption isotherm measurements). The thermal desorption rate coefficient of a molecule is related to the time a transiently adsorbed molecule resides on a surface. The surface site density is the total number of molecules per unit area on a surface completely covered with a layer of adsorbate one molecule thick (a "monolayer").

Desorption rates, adsorption isotherm, and photodeposition rates were measured using the two model contaminants: DC-704 and DEHP. The range of molecular arrival rates selected for the desorption, adsorption, and photodeposition experiments was based on the data obtained from model calculations done by the manufacturer of the SDS vehicle. These calculations estimated that the molecular arrival rate on the satellite surfaces was about 1 nm h^{-1}. Most of the experiments discussed in this report were conducted in the range of 0.2 to 2 nm h^{-1}. The procedures used to measure these rates are described subsequently.

1. DESORPTION RATES

The desorption rate coefficient, k_2 (see Appendix B), was measured by adsorbing about a monolayer of DEHP or DC-704 onto the TQCM surface. (A monolayer is a mass density equivalent to approximately 2 nm of uniform film.) Once the desired amount of contaminant was deposited, the apparatus shutter was closed, and the crystal frequency was measured as a function of time. The DC-704 desorption rate was measured from an aluminum surface with photodeposit on it (termed exposed surface). The DEHP desorption rate coefficient was measured from two surfaces: a platinum surface that was not contaminated by photodeposit and a platinum surface that had photodeposit on it.

2. STEADY-STATE ADSORPTION ISOTHERM

The steady-state adsorption isotherm measurements were performed by first adjusting the Knudsen cell temperature and TQCM temperatures to the desired levels. The apparatus shutter was then opened, and the molecular contaminant was adsorbed onto the TQCM until the rate of frequency change was zero. A series of measurements was made at various molecular arrival rates at constant TQCM temperatures. The arrival rates were adjusted to low values to keep the TQCM surface coverage below a monolayer and thus to minimize effects resulting from bulk adsorption.

3. PHOTODEPOSITION RATES

Photodeposition rates were measured in a carefully orchestrated sequence to eliminate possible false readings caused by temperature fluctuations and light interactions with the TQCM. A typical experiment began with the measurement of TQCM interactions in the dark with the molecular beam for 48 h. The VUV lamp was then turned on, and the beat frequency was measured for enough time to provide an adequate signal-to-noise ratio, typically about 48 h (see Appendix A). In spite of attempts to provide uniform illumination of the sample and reference electrodes of the TQCM, a transient perturbation of the beat frequency was often seen when the VUV light was turned on or off.

During photochemical deposition experiments, the TQCM was surrounded with passive witness samples of various materials which were used for ex situ spectroscopic analyses of the deposited films. These witness samples also provided a test of the effect of substrate identity on deposition rate.

III. RESULTS

The results of the desorption, steady-state adsorption isotherm, and photodeposition experiments are presented in this section.

We found that the thermal desorption rates of the DC-704 and DEHP contaminants could be well described by a first order rate coefficient that depends on substrate temperature in an Arrhenius fashion. These model contaminants resided on clean and contaminated surfaces at about 304 K (without illumination) for about 10^2 sec.

The steady-state adsorption isotherm and photodeposition experiment results supported the hypothesis that photochemical contaminant deposition is a competition between photolysis and desorption of a transiently adsorbed contaminant molecule. The contaminant deposition rate was inversely dependent on substrate temperature. Both photodeposition rate measurements and analysis of witness samples (small coupons of various material used to determine substrate effects on photodeposition) revealed that the absolute rate of film accretion depends on the type of substrate and on the precursor molecule.

A. DESORPTION RATES

First order desorption kinetics were observed. Figure 6 shows a typical desorption plot--ln(mass) versus time, for DEHP-- from which a value of k_2 is obtained. The interaction energy between the surface and the DEHP was determined by measuring k_2 from a series of desorption experiments conducted at various substrate temperatures. The rate coefficient was found to depend on substrate temperature in an Arrhenius fashion ($k_2 = A \exp[E_a/RT]$) (see Figs. 7 and 8). The desorption energies and pre-exponential factors obtained from the plots in Figs. 7 and 8 are listed in Table 1.

The desorption energy for DEHP appears to approach the bulk heat of vaporization[10] of 26.3 kcal $mole^{-1}$ as the surface becomes covered with

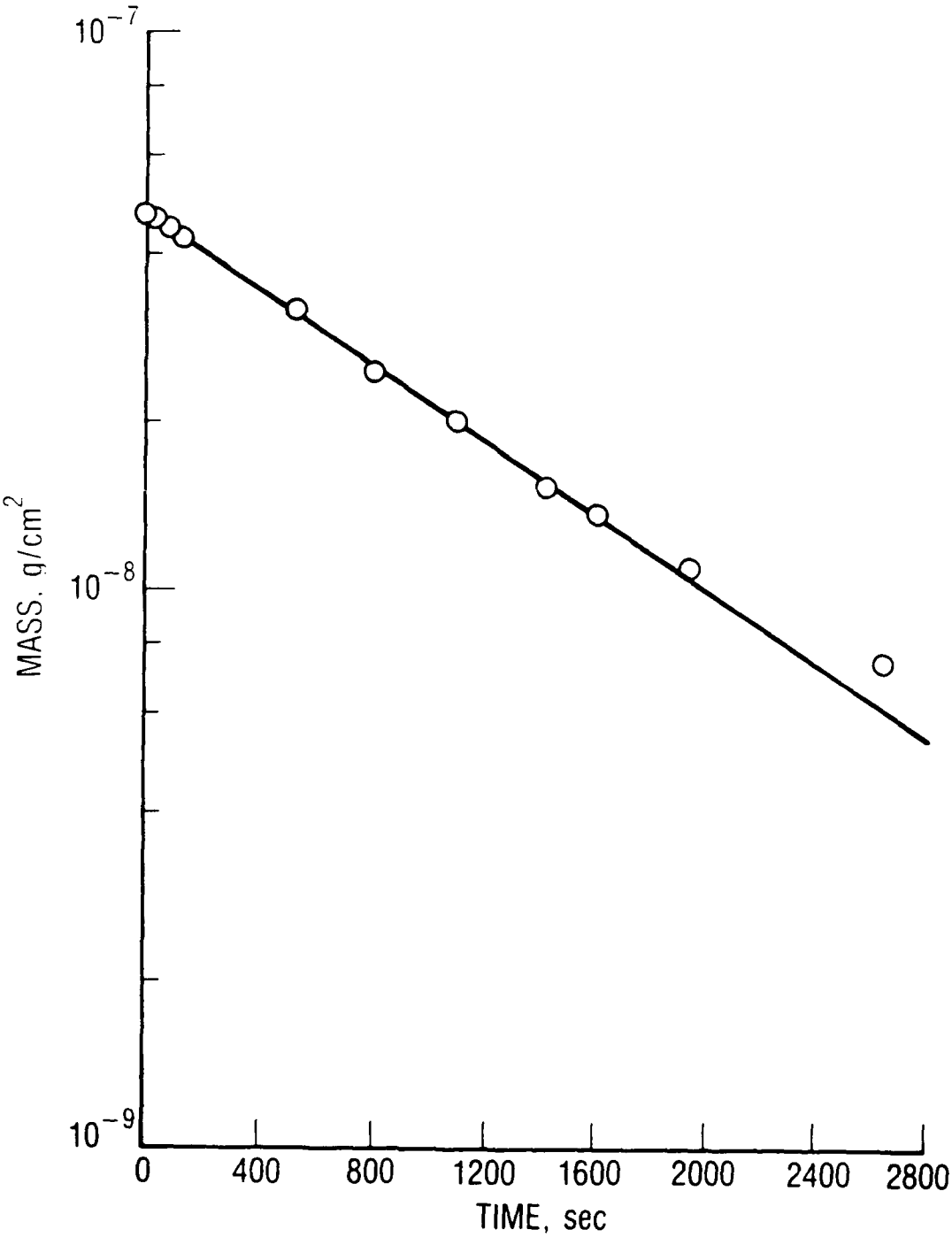

Fig. 6. First Order Kinetic Plot of Desorption of DEHP from a Quartz Crystal Microbalance Surface. The straight line is a linear least-squares fit, the slope of which is the rate coefficient for desorption at the temperature of the experiment.

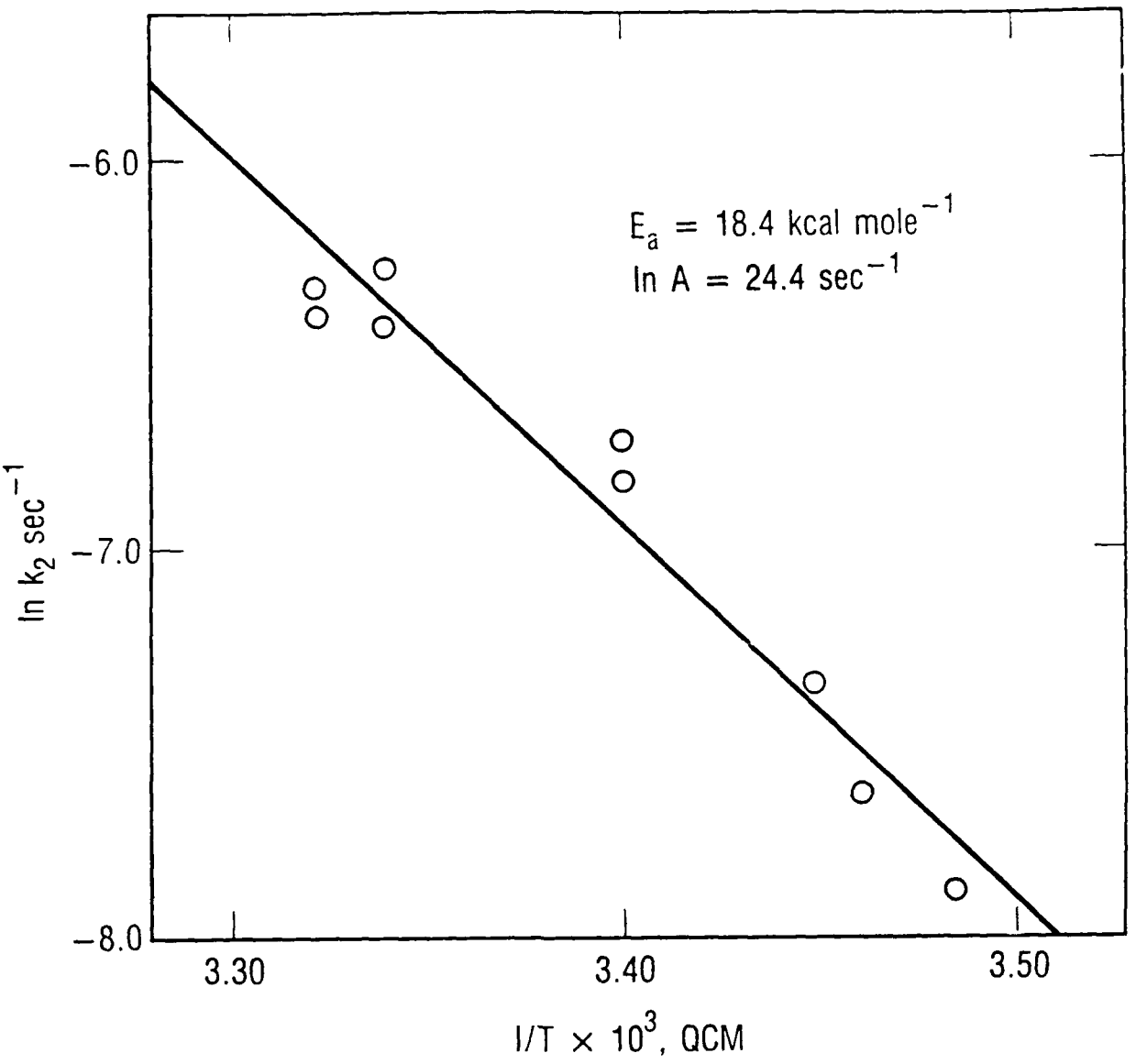

Fig. 7. Arrhenius Plot (in Substrate Temperature) of the Thermal Desorption Rate of DC-704 from a Quartz Crystal Microbalance Surface

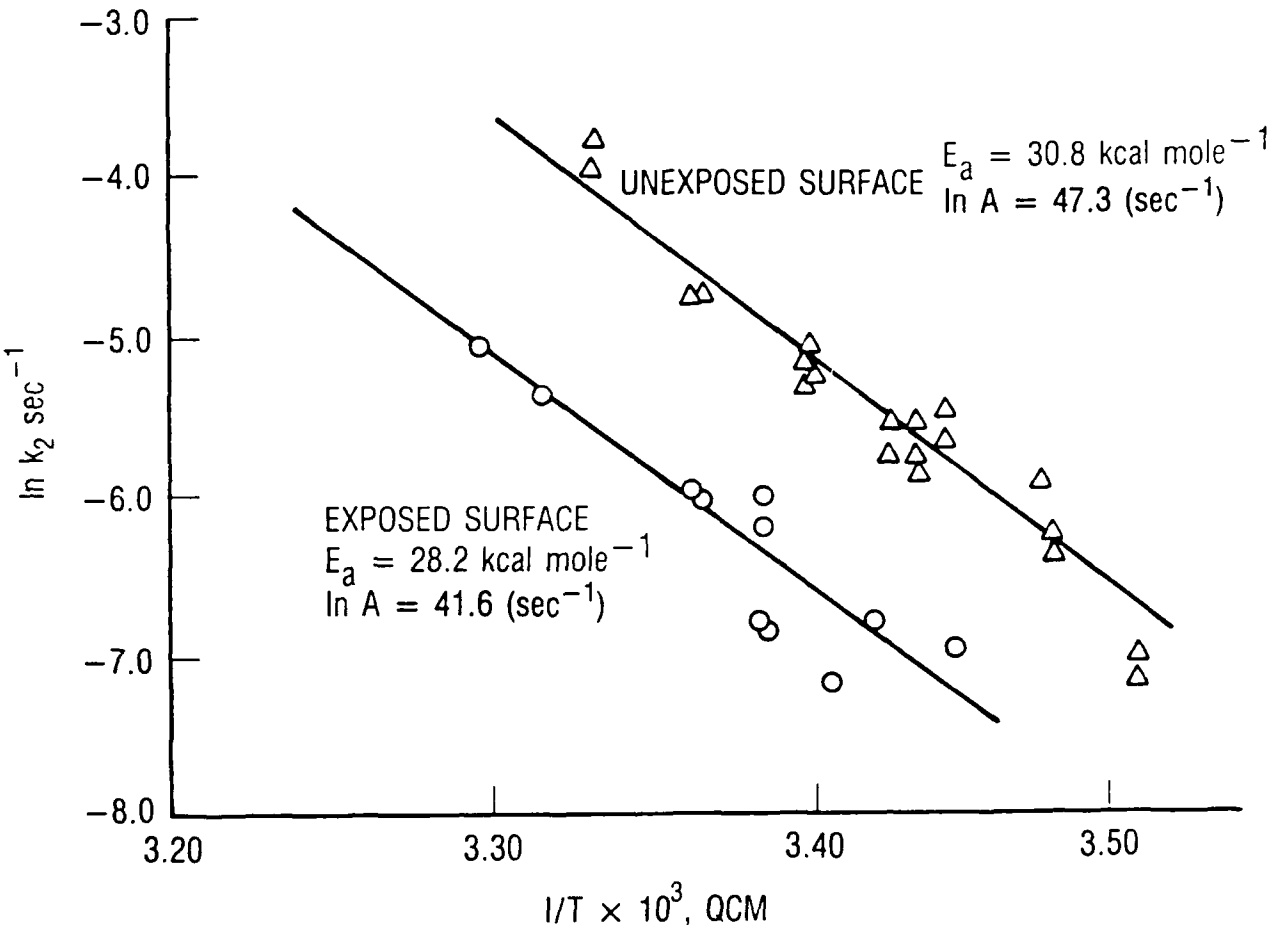

Fig. 8. Arrhenius Plot (in Substrate Temperature) of the Thermal Desorption Rate of DEHP from a Quartz Crystal Microbalance Surface

deposit. The bulk heat of vaporization for DC-704 is 25.8 kcal $mole^{-1}$.[11] The desorption energy for DC-704 is somewhat lower than the heat of vaporization, which would indicate that the interaction energy between the contaminated surface and the adsorbed DC-704 is less than the interaction energy between molecules in the bulk.

Table 1. Arrhenius Parameters for Thermal Desorption of DC-704 and DEHP from Quartz Crystal Microbalance Surfaces

Material	Surface	E_a (kcal $mole^{-1}$)	ln(A) (sec^{-1})
DC-704	Al (exposed)	18.4	24.4
DEHP	Pt (exposed)	28.2	41.6
DEHP	Pt (unexposed)	30.8	47.3

Table 2 shows the rate coefficients computed from the Arrhenius parameters in Table 1. The rate of photochemical film deposition was measured on unexposed aluminum, exposed platinum, and unexposed platinum.

Table 2. Computed Thermal Desorption Rate Coefficients for DC-704 and DEHP at Temperatures Used in Isothermal Contaminant Deposition Experiments

Contaminant	Substrate	Substrate Temperature (K)	k_2 (sec^{-1})
DC-704	Al (exposed)	306	2.9×10^{-3}
DEHP	Pt (exposed)	302	4.5×10^{-3}
DEHP	Pt (unexposed)	302	1.8×10^{-2}

The mean residence time for a molecule on the temperature-controlled quartz crystal microbalance (TQCM) surface is approximately the inverse of the desorption rate coefficient. Thus, at these temperatures, the lifetime of DC-704 on a contaminated surface is about 300 sec. The lifetimes of DEHP are about 200 and 50 sec for the exposed and unexposed platinum surfaces, respectively.

B. STEADY-STATE ADSORPTION ISOTHERM EXPERIMENT

Figure 9 exhibits the slopes of DEHP steady-state adsorption isotherm measurements for exposed and unexposed platinum surfaces. The slopes of these "Langmuir" plots indicate the surface site density (S_0), and the intercept indicates k_2 (see Appendix B). The results for DEHP on platinum are given in Table 3. The results indicate reasonable agreement with the desorption experiment. The desorption rate coefficients are much lower on the exposed surface than on the unexposed surface.

Table 3. Site Densities and Thermal Desorption Rate Coefficients for DEHP Adsorption Inferred from Steady-State Adsorption Isotherm Experiments

Surface	Temperature (K)	Site Density (cm^{-2})	k_2 sec^{-1}
Exposed Pt	302	1.4×10^{14}	1.7×10^{-3}
Unexposed Pt	302	5.8×10^{13}	1.8×10^{-2}

C. PHOTODEPOSITION RATES

A plot of the data taken during a typical experiment is presented in Fig. 10. The model for the photodeposition process, presented in Appendix B, predicts that a plot of the inverse deposition efficiency, e

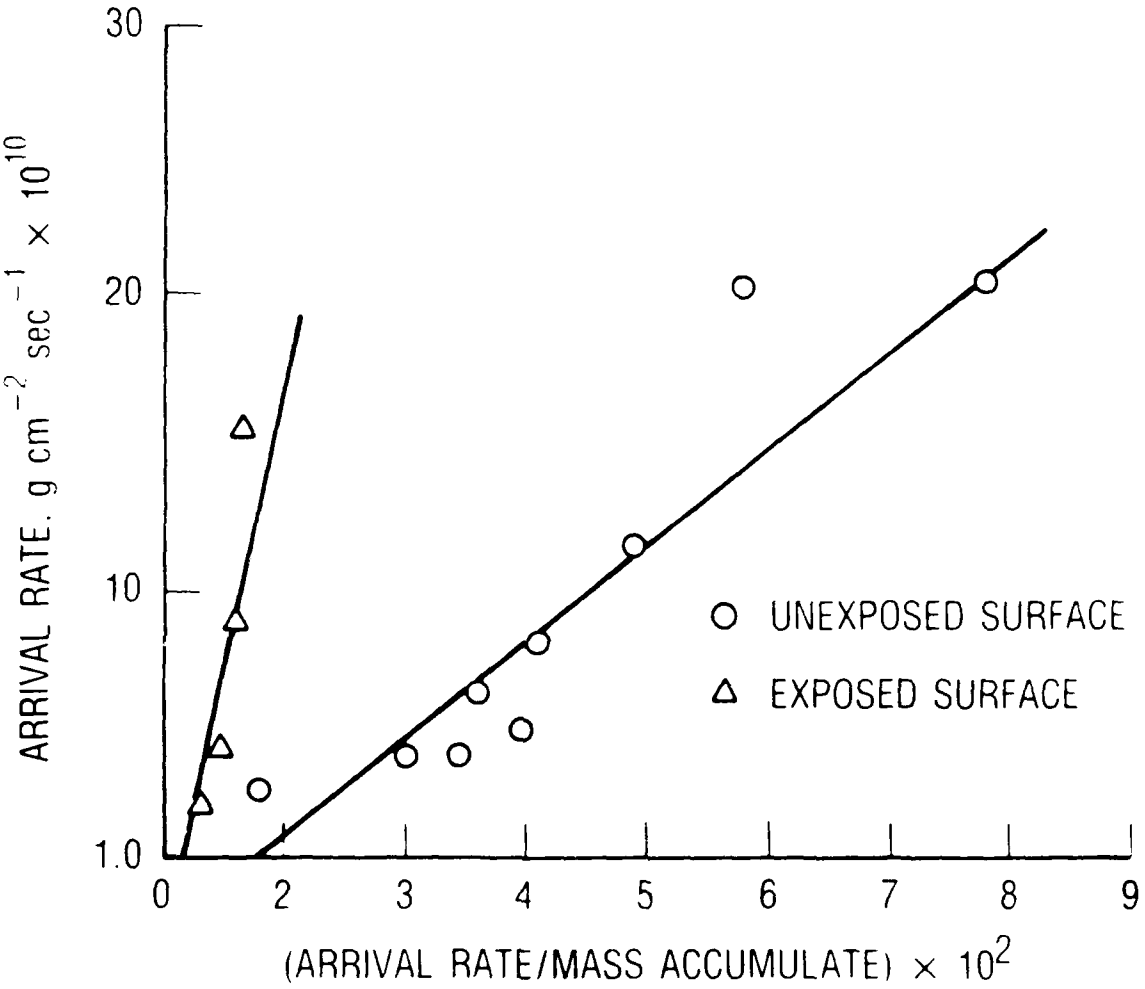

Fig. 9. "Langmuir" Plot of Steady-State Mass Accumulation of DEHP on a (Dark) Quartz Crystal Microbalance Surface

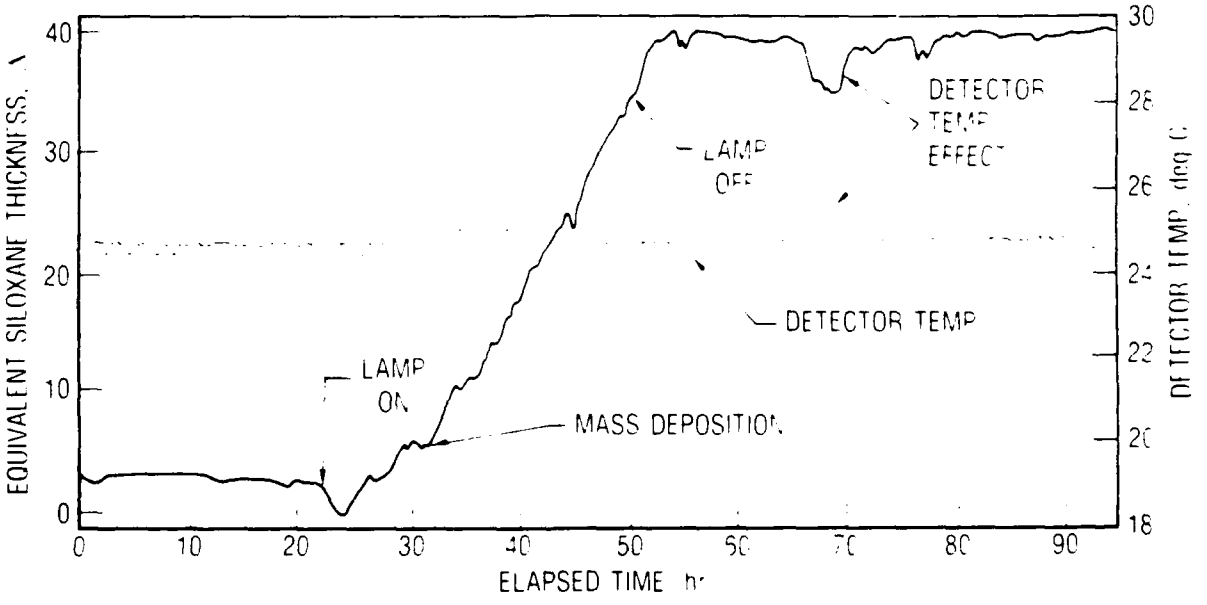

Fig. 10. Typical Photochemical Deposition Data

(accretion rate/arrival rate), versus the arrival rate, F_c, should give a straight line with a slope equal to $(k_3qI_0S_0)^{-1}$. The intercept should be equal to $(k_2 + k_3qI_0)/k_3qI_0P_0$, where k_3q is the effective photochemical cross section, I_0 is the light intensity, P_0 is the clean surface sticking coefficient, and S_0 is the effective site density. Figures 11 and 12 show plots of e^{-1} versus F_c for DC-704 and DEHP, respectively. We have assumed for these calculations that the mass of the deposit molecule is approximately equal to the mass of the contaminant molecule.

Table 4 presents the results of a linear regression analysis of the photodeposition data taken at constant temperature. The expression for the intercept b can be rearranged to produce

$$k_3q = k_2/[I_0(bP_0 - 1)] \qquad (1)$$

Because all the parameters in Eq. (1) are uniquely positive, there is a minimum value for P_0, depending upon the intercept value obtained for each contaminant. For DC-704, P_0 has a minimum value of 0.64; for DEHP, P_0 has a minimum value of 0.13. These minimum values correspond to the physically unreasonable case of an infinite effective absorption cross section. The true values of P_0 must be larger than these minimum values. The relatively large values of the lower limits support the choice of $P_0 = 1$ in subsequent analyses.

Table 4. Linear Regression Results for the Flux Dependence of the Photochemical Contaminant Deposition Rate

Material	Substrate Temperature (K)	Slope (10^{-10} cm^{-2} sec)	Intercept (Unitless)	Correlation Coefficient
DC-704	306	2.86	1.56	0.93
DEHP	302	2.98	7.7	0.98

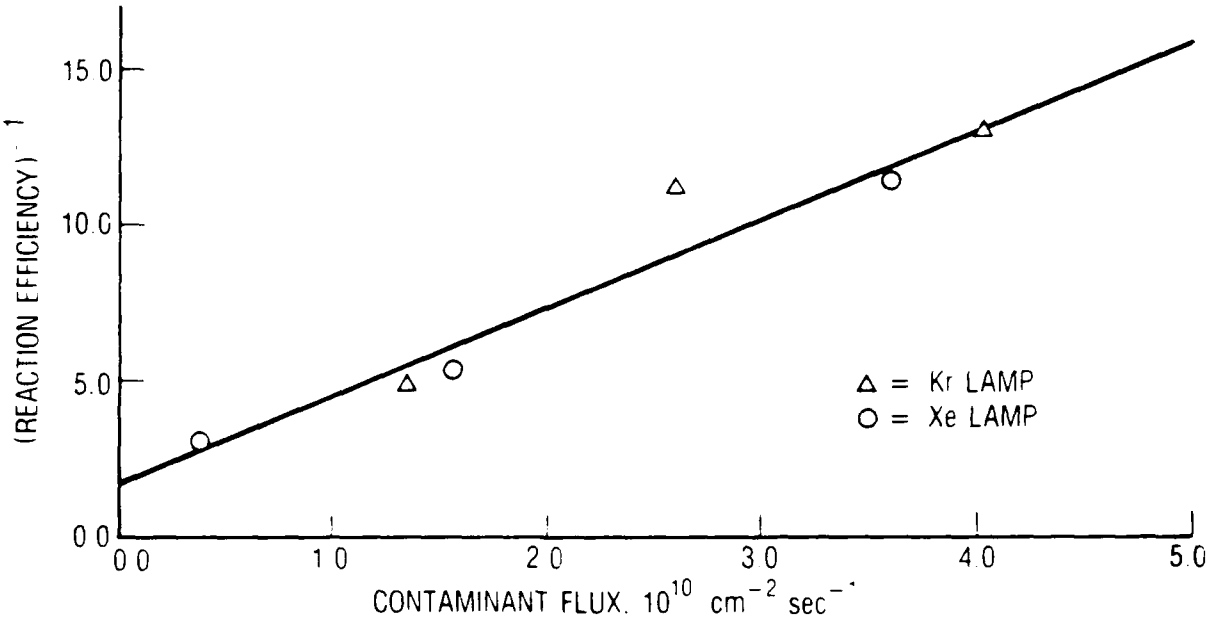

Fig. 11. Plot of the Reciprocal of the DC-704 Isothermal Photochemical Deposition Efficiency versus the Incident Flux. The solid line is a linear least-squares fit.

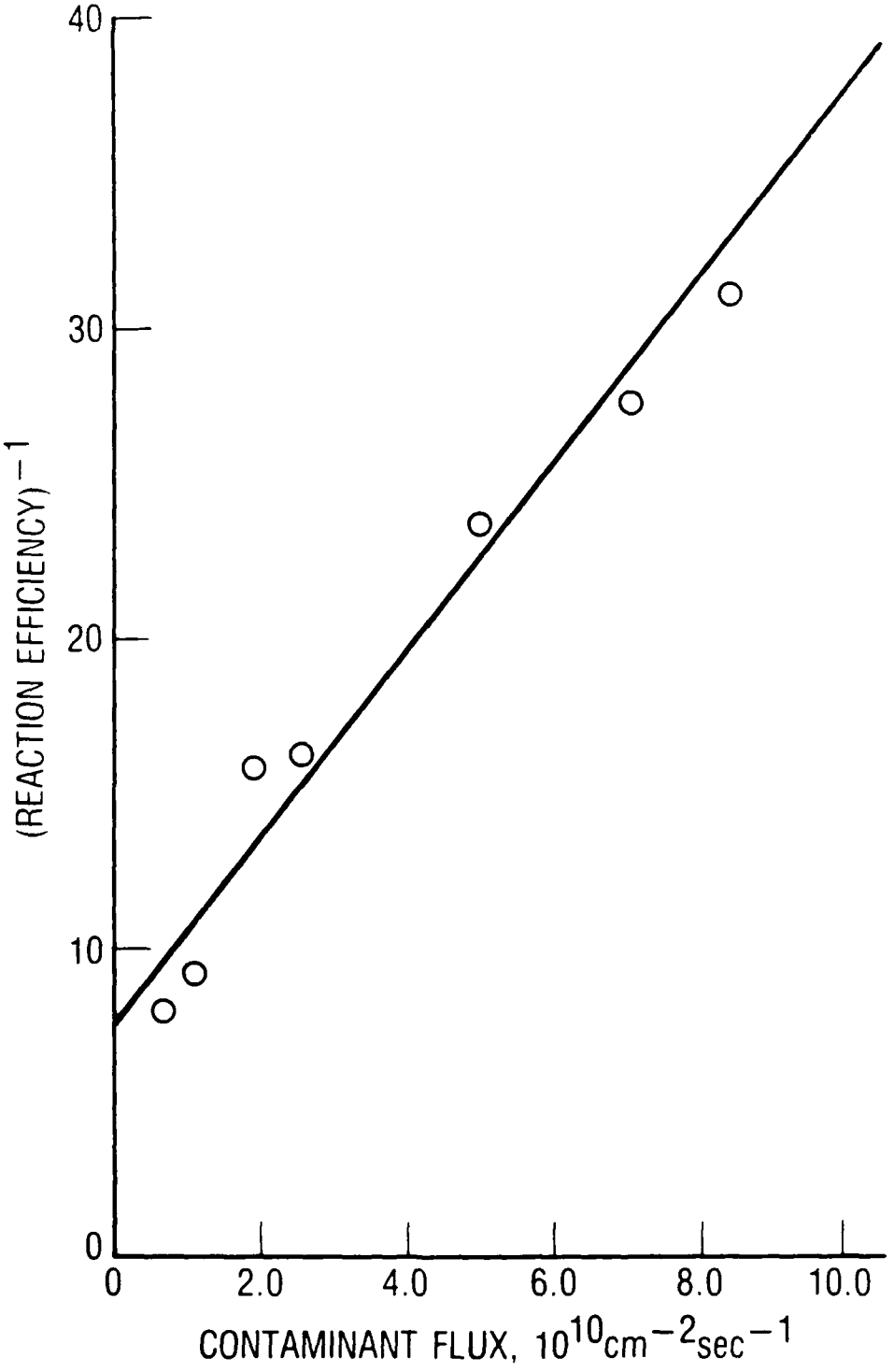

Fig. 12. Plot of the Reciprocal of the DEHP Isothermal Photochemical Deposition Efficiency versus the Incident Flux. The solid line is a linear least-squares.

Using the independently measured values of k_2, and assuming that $P_0 \cong 1$, one may calculate k_3q and S_0 from the slope and intercept values in Table 4. Two values for the site density for DEHP were calculated. Each value was based on a different value for k_2 obtained from the desorption and steady-state adsorption isotherm experiments for an exposed surface. These values are listed in Table 5.

Table 5. Site Densities and Effective Absorption Cross Sections Inferred from the Flux Dependence of the Photochemical Contaminant Deposition Rate

Material	k_2 sec^{-1}	Site Density S_0 (cm^{-2})	k_3q (cm^2)
DC-704	2.9×10^{-3}	6.8×10^{11}	7.5×10^{-16}
DEHP[a]	4.5×10^{-3}	5.7×10^{12}	9.7×10^{-17}
DEHP[b]	1.7×10^{-3}	1.3×10^{13}	3.7×10^{-17}

[a] k_2 values obtained from exposed surface isothermal desorption measurement.

[b] k_2 values obtained from steady-state adsorption isotherm measurement.

Recall that the quantity k_3q is the effective absorption cross section of the adsorbed contaminant. The absorption cross section determined for DC-704 is approximately equal to the bulk absorption cross section at this wavelength range (130-190 nm).[12] No such values for DEHP are known in the VUV region; however, a comparison of DEHP to polystyrene may be appropriate because these molecules are quite similar in structure, except that no carbonyl groups are present in polystyrene. The absorption cross section for polystyrene is 5×10^{-17} cm^{-2} at 180 nm.[13] This value is quite close to the DEHP values if $q \cong 1$. One would expect the absorption cross sections for these two molecules to be quite similar in this wavelength region because light absorption excites electrons in the pi orbitals. The

densities of the two molecules are approximately the same; therefore, the numbers of phenyl groups per unit area of the two molecules will be approximately the same. At the shorter wavelengths (130-150 nm), the absorption occurs primarily in the C-C and C-H bonds. The absorption bands of DEHP are extended somewhat further to the near UV because the carbonyl group is conjugated with the pi orbitals in the phenyl ring.

The rate of deposition does not appear to be particularly sensitive to the wavelength of radiation below 200 nm. In Fig. 11, the data plotted for DC-704 were taken with two light sources of approximately equal flux, krypton and xenon lamps. Deposition was not observed for illumination at wavelengths greater than 200 nm.

The photodeposition rate was found to be dependent upon the substrate temperature. Figures 13 and 14 present Arrhenius plots in substrate temperature of the deposition rate for DC-704 and DEHP. The apparent activation energy for DC-704 over the temperature range of 298 to 323 K is -13.5 kcal $mole^{-1}$ and for DEHP over the temperature range of 285 to 313 K is -26.8 kcal $mole^{-1}$. (Of course, these activation energies are valid only over the measured temperature range. Unlike a positive activation energy, a negative activation energy cannot prevail in the limit of low temperature.)

D. EFFECT OF SUBSTRATE IDENTITY

The X-ray photoelectron spectroscopy (XPS) spectra of the witness samples exposed to DC-704 in the absence of radiation indicated less than one monolayer of silicon. The XPS spectra of vacuum ultraviolet (VUV) irradiated samples indicated a considerable amount of silicon. The amount of silicon on the irradiated samples depended on the substrate material: substantial silicon was present on the magnesium fluoride and aluminum surfaces but not on the gold surfaces. The samples were exposed to the molecular beam at a rate of 0.4 nm h^{-1} for 50 h. The XPS spectra for the exposed samples give a lower limit on the thickness of 6 nm. The lower limit of the film thickness can be determined by the attenuation of the

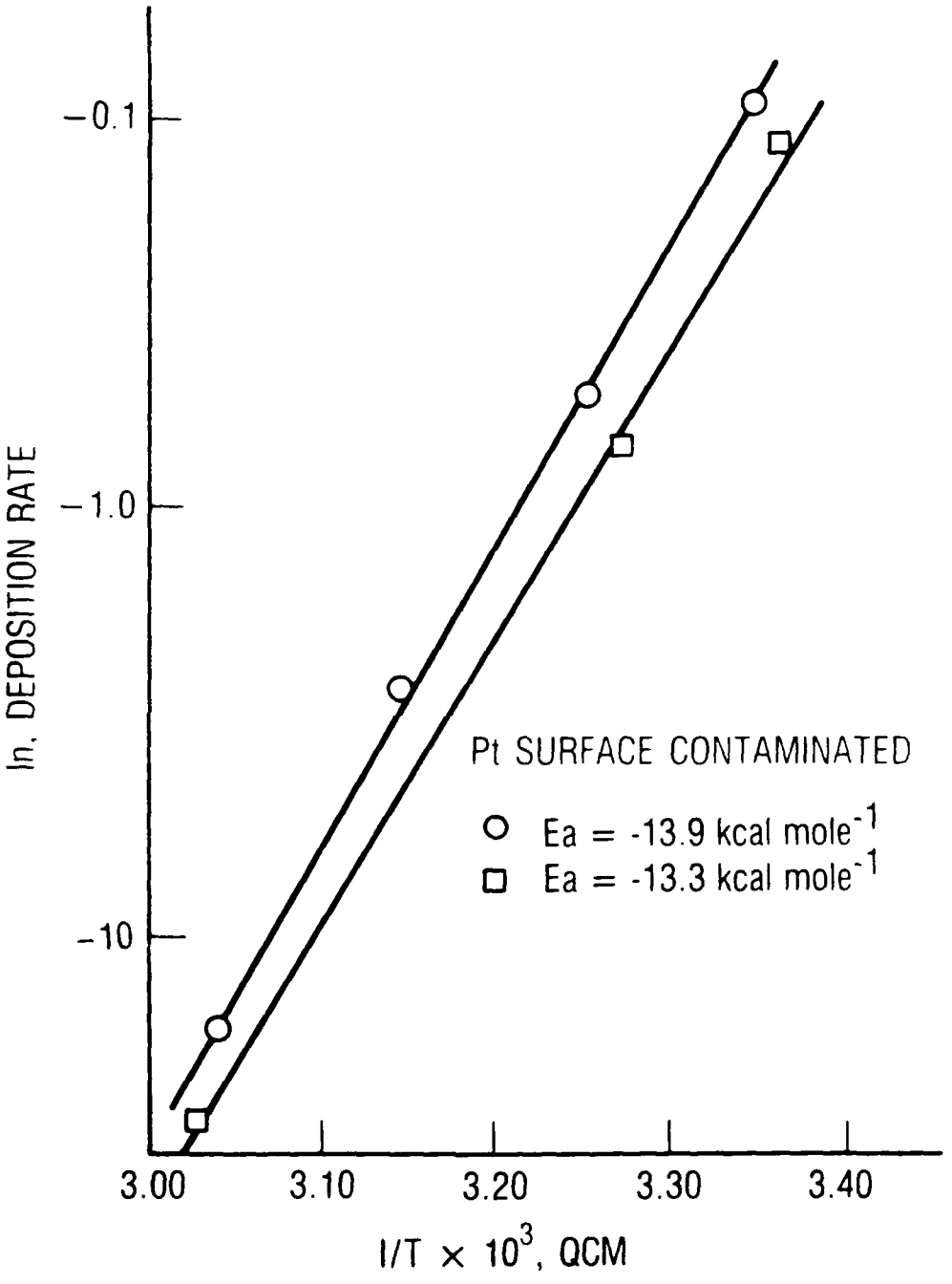

Fig. 13. Arrhenius Plot (in Substrate Temperature) of the DC-704 Photochemical Deposition Rate at Constant Incident Flux

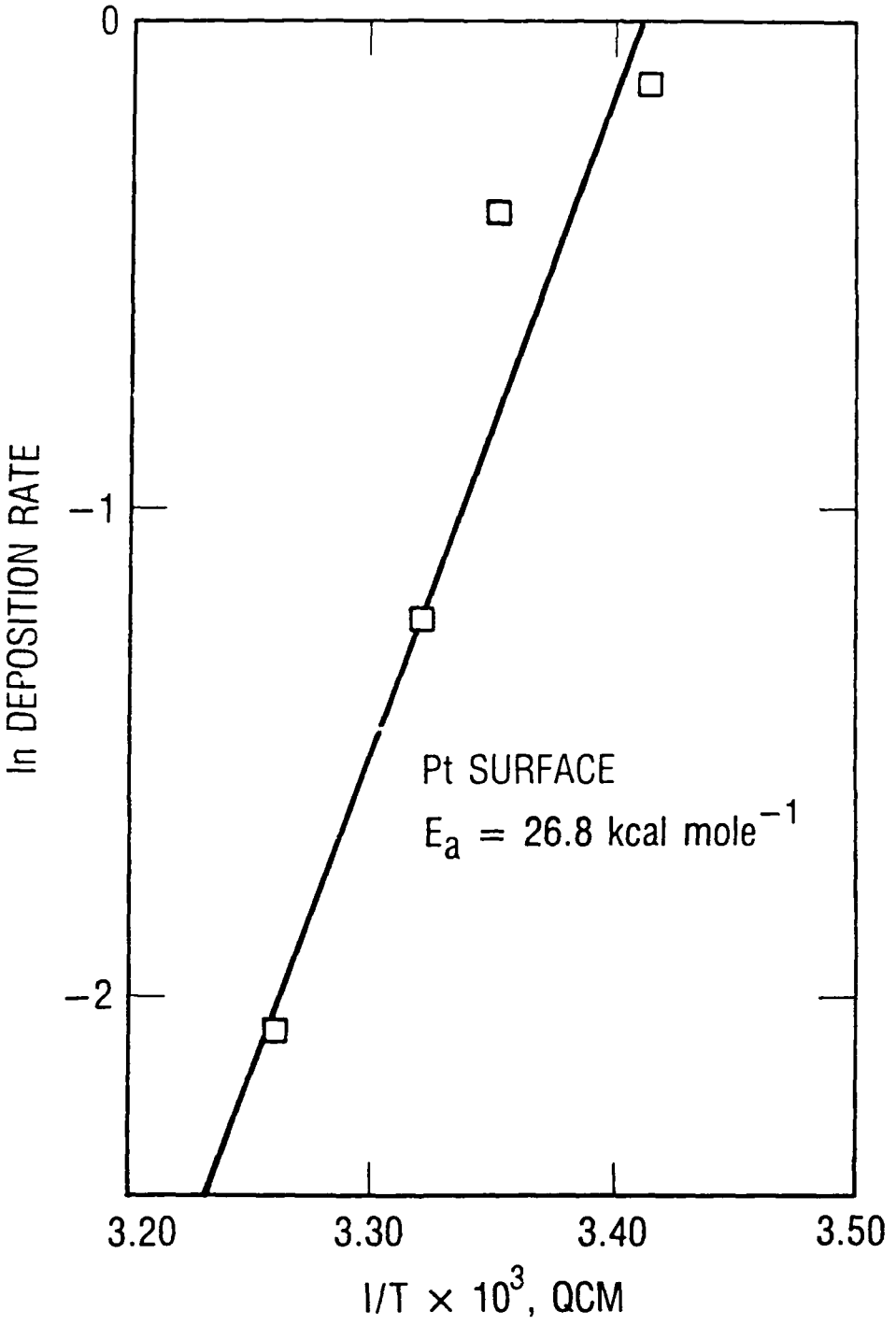

Fig. 14. Arrhenius Plot (in Substrate Temperature) of the DEHP Photochemical Deposition Rate at Constant Incident Flux

magnesium photoelectron signal by the contaminant overlayer. (If the deposition efficiency were unity, a film of about 20 nm would have formed.) The silicon thickness on the background sample was less than 1 nm.

XPS also revealed that the oxidation state of silicon had changed as a result of the exposure of DC-704 to VUV. For silicon in DC-704, the binding energy of the photoelectron was measured to be 101.1 eV; in silicon dioxide, the binding energy is 103 eV.[14] The irradiated samples exhibited a binding energy of 102.2 eV, midway between that of DC-704 and SiO_2. The result clearly indicates that the silicon has undergone a chemical reaction in which the oxidation state of the atom has increased. The photolysis has apparently removed some methyl and phenyl groups and increased the number of silicon-oxygen bonds, resulting in a higher oxidation state. This conclusion is supported somewhat by the UV spectrum of the irradiated deposit. The removal of methyl (CH_3) groups has been observed by Siegel and Stewart in their work on the VUV photolysis of bulk DC-704.[15]

Auger analysis of the split witness samples graphically illustrated the effect of substrate composition on the amount of contaminant deposited. These samples were analyzed by Auger depth profiling, during which the film on the substrate was systematically removed by ion milling using 3 keV argon ions. The results of one measurement of photodeposits on gold and aluminum witness samples are shown in Fig. 15. The difference between the sputter times for the silicon signal to reach zero on gold and on aluminum is quite striking and clearly supports the belief of a substrate effect on the deposition rate. The estimated film thicknesses, based on the sputter times, are approximately 4 and 23 nm for the gold and aluminum surfaces, respectively. The witness samples were exposed to the molecular contaminant for 203 h at a molecular arrival rate of 0.44 nm h^{-1}. Therefore, this measurement suggests that the photodeposition efficiency appears to have averaged about 0.3 for aluminum. These films were deposited during studies measuring the effect of substrate temperature on the contaminant deposition rate. Thus the deposition efficiency is the deposition time-weighted average for many different substrate temperatures.

In Fig. 15 the initial silicon signal on gold appears to be the same intensity as the silicon signal on aluminum, thus giving the impression that the contaminant concentration is the same on both surfaces. This is not the case. The Auger analysis enhances the signal of films on substrates with high Z (atomic numbers) relative to substrates with low Z. The high Z of gold (Z = 79) relative to the low Z of aluminum (Z = 13) means a relative signal enhancement of about a factor of 2 or 3 for silicon on the gold substrate. Thus, the difference in the initial concentrations of DC-704 photodeposit on gold and aluminum is greater than it appears to be from the depth profiles.

Auger electron spectroscopy (AES), and not XPS, detected silicon on gold because the witness samples analyzed by AES were exposed for much longer times to the contaminant and VUV fluxes and because AES is a more sensitive technique.

The effect of substrate composition on the contaminant deposition rate of DC-704 was also demonstrated by measuring the rate of deposition on gold and platinum TQCM electrodes. The rate of deposition was measured with both substrates at 305 K and exposed to xenon radiation. The results are shown in Table 6. The deposition rate is about a factor of 3 higher on the platinum surface than on the gold surface, and the deposition efficiency is about a factor of 4 higher on the platimum surface.

E. ULTRAVIOLET AND INFRARED ABSORPTION SPECTRA OF PHOTODEPOSITS

UV and visible absorption spectra of the photodeposits were measured and compared to the absorption spectra of unphotolyzed molecules. Figure 16 is the spectrum of the irradiated deposit from DC-704 collected on the sapphire window that covered the TQCM reference electrode. Figure 17 is the spectrum of the unirradiated DC-704. Note that the absorption edge of the irradiated material extends well into the near UV region and that there is a loss of structure in the UV region. The deposit appeared yellowish brown, indicating some adsorption in the visible portion of the spectrum. This loss of structure indicates photolysis of phenyl

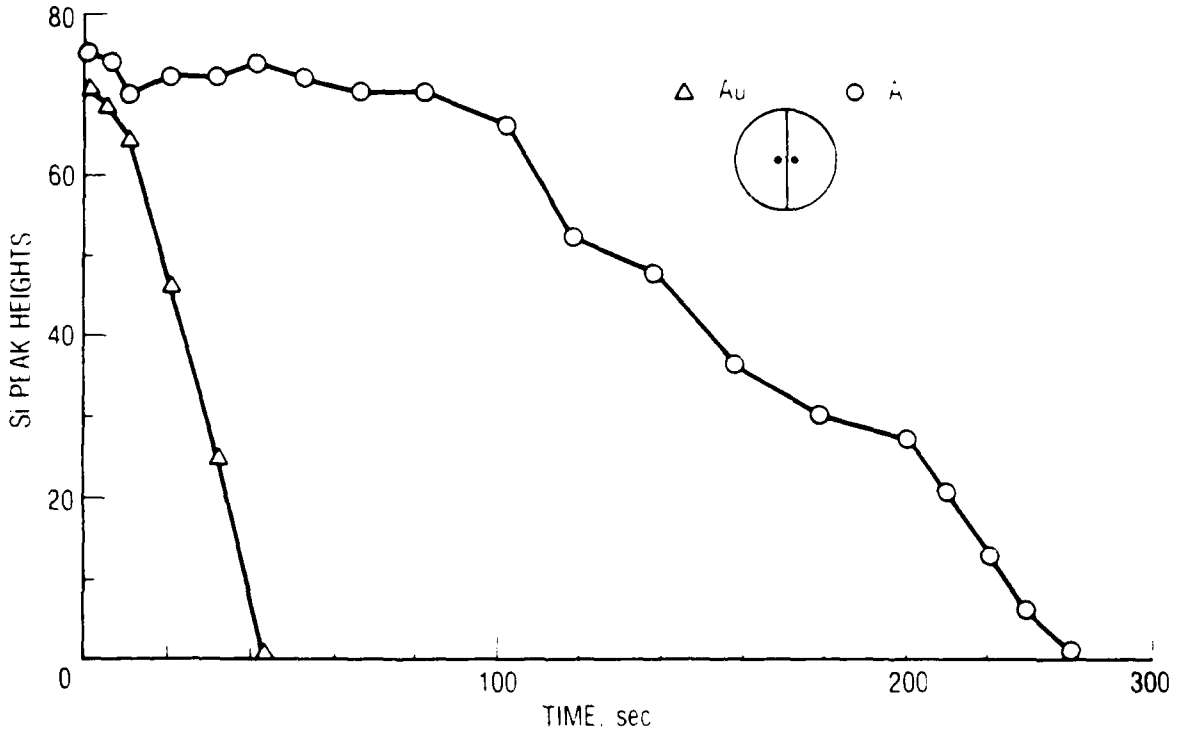

Fig. 15. Auger/Sputtering Depth Profile of Silicon on DC-704 Photocontaminated Gold and Aluminum Witness Samples

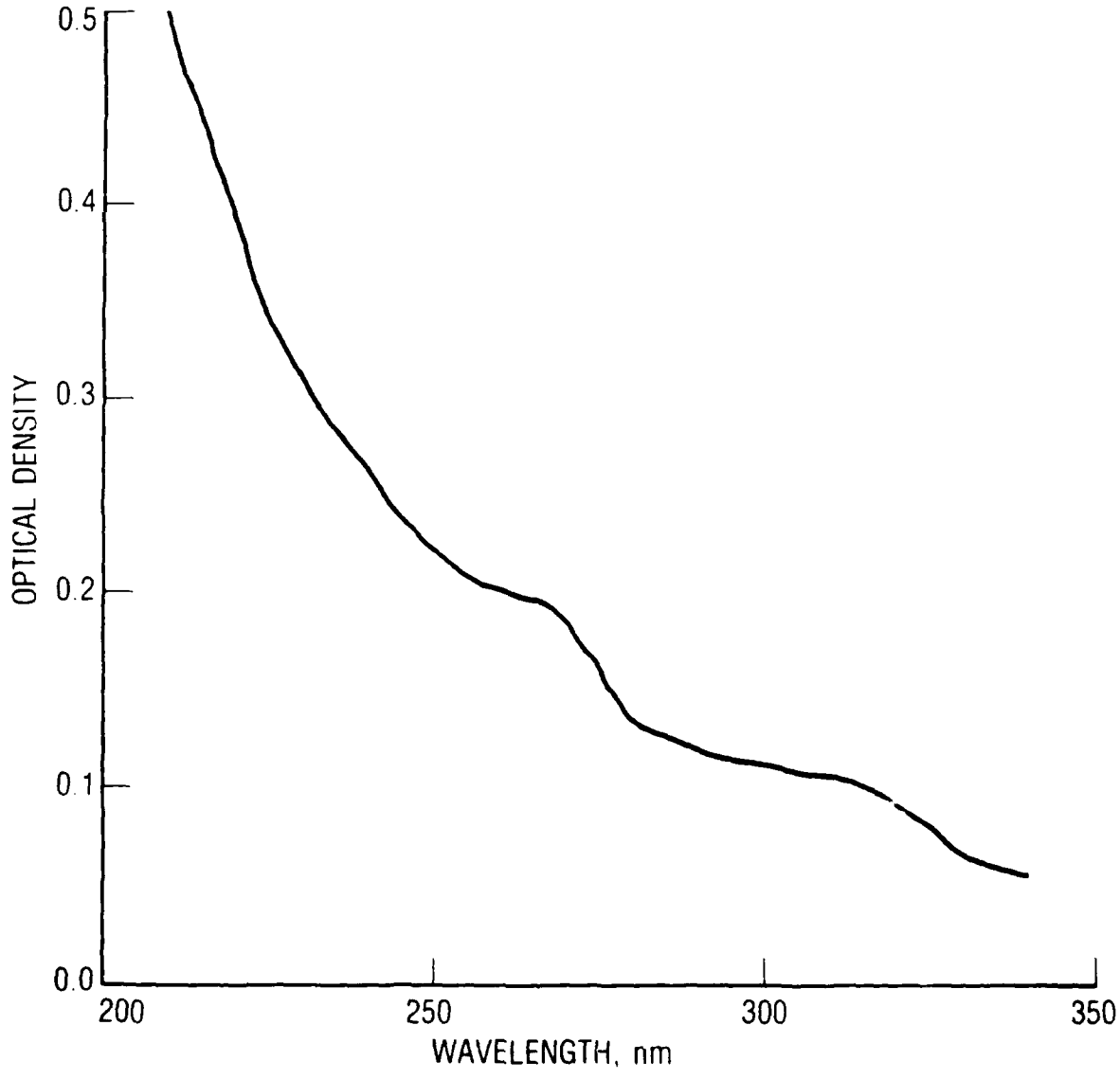

Fig. 16. Near Ultraviolet Absorption Spectrum of the Photodeposit from DC-704 on a Sapphire Substrate. Assignment of an absolute absorption coefficient for the contaminant is not possible because the deposit thickness is unknown.

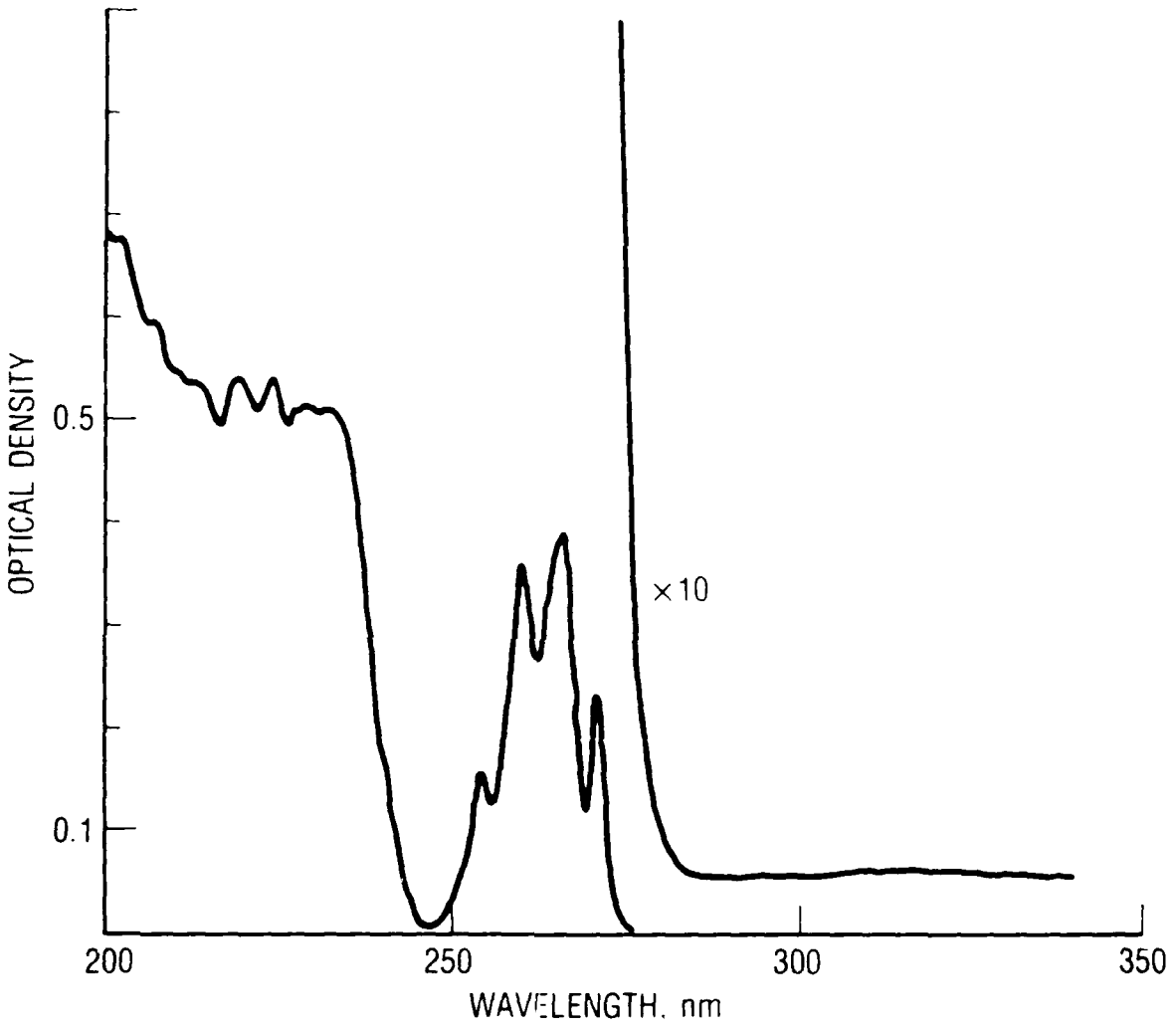

Fig. 17. Near Ultraviolet Absorption Spectrum of DC-704

Table 6. Substrate Effect on the Photochemical Contaminant Deposition[a]

Substrate	Flux (nm/h)	Temperature (K)	Deposition Rate (nm/h)	Efficiency
Au	0.58	309	0.016	0.027
Au	0.58	304	0.027	0.047
Au	0.64	308	0.027	0.041
Pt	0.44	306	0.096	0.22
Pt	0.44	308	0.084	0.19

[a]Xenon irradiation.

groups on the DC-704 molecule, resulting in the formation of some carbonaceous material. No spectrum was obtained for the deposits from the phthalate compounds. The assignment of an absolute absorption coefficient for the contaminant on the sapphire window is difficult because the deposit thickness is not known, since the deposit is a sum of the depositions from many runs performed at different temperatures.

The infrared (IR) absorption spectrum of DC-704 photodeposit on silicon is shown in Fig. 18. For comparison, Fig. 19 shows the spectrum of an Si blank with no radiation exposure. The presence of photoinduced deposits on the silicon surface is seen by the presence of Si-O bonds, as indicated by the strong band at 1050 cm^{-1}; by methyl groups ($-CH_3$) with bands at 1300 and 2950 cm^{-1}; by an Si-phenyl band at 1300 cm^{-1}; and by one interesting band at 1720 cm^{-1}, which is the result of a carbonyl group. The formation of the carbonyl group, which is not present in DC-704, is probably the result of the reaction of a photoactivated species with oxygen in the atmosphere when these samples are exposed to air.

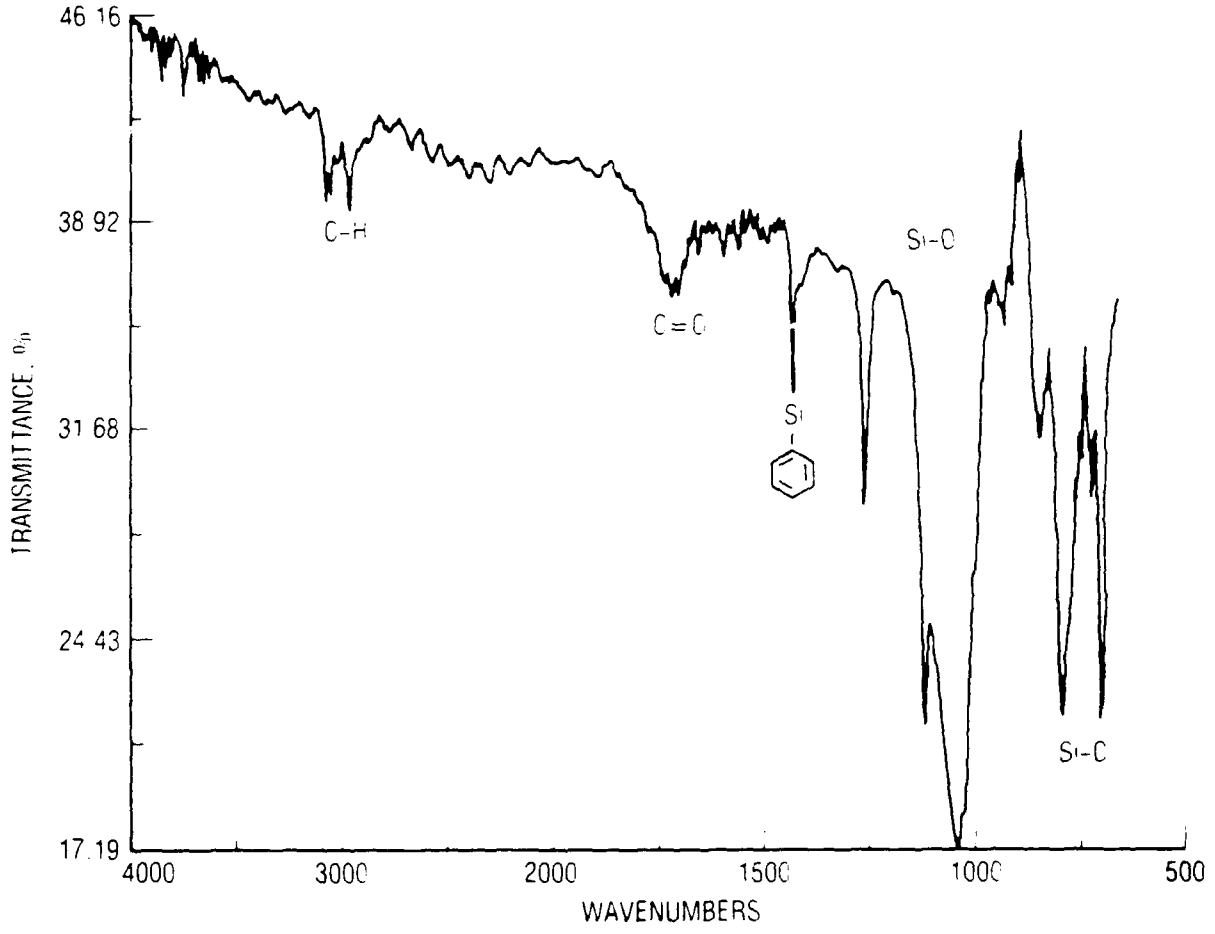

Fig. 18. Infrared Absorption Spectrum of DC-704 Photodeposit on Silicon

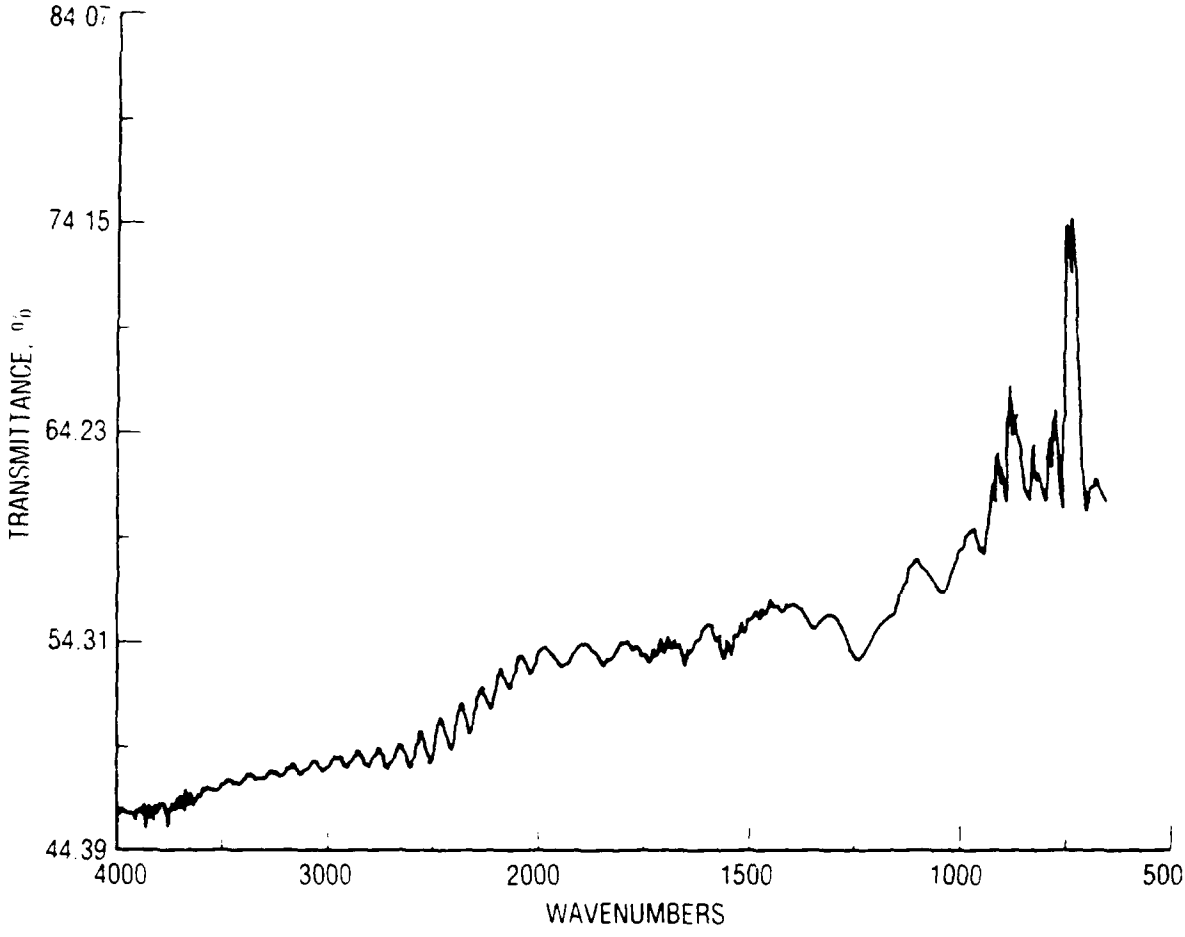

Fig. 19. Infrared Absorption Spectrum of an Unirradiated Silicon Substrate

IV. DISCUSSION

Absolute rates for vacuum ultraviolet (VUV) deposition of organic films representative of spacecraft contaminants have been measured. In the first section of this discussion, we show that the measured deposition rates are large enough to explain a real space vehicle anomaly. The second section describes a very simple kinetic model, based on a competition between desorption and photolysis of a transiently adsorbed precursor molecule. The model, which uses experimentally measured parameters, is reasonably successful in describing the photodeposition process. In the final section we compare the results of these laboratory expriments with those of the SCATHA ML-12 spaceflight experiment.

A. COMPARISON OF RESULTS WITH SATELLITE DATA SYSTEM RADIATOR DEGRADATION

This work was undertaken to ascertain whether photochemical film deposition could explain the unexpectedly high increase in solar absorptance of the Satellite Data System (SDS) satellite radiator. The question was not whether VUV photochemical deposition of large organic molecules occurs but whether the absolute deposition rate is large enough to account for the observed radiator degradation. It was estimated that the satellite radiator surface in question experienced a total molecular flux of less than 0.4 $\mu g\ cm^{-2}\ h^{-1}$. The relative temperatures of the molecular sources and collectors (i.e., the radiators) were such that condensation was not expected to occur. A contaminant deposition rate of approximately 1 $ng\ cm^{-2}\ h^{-1}$ was necessary to explain the rate of increase in solar absorptance of the vehicle radiator.

The initial investigations by Hayes[1] were performed with fluxes of molecules (outgassing from spacecraft engineering materials) much higher than this expected value. If one extrapolated Hayes's results linearly to the appropriate molecular arrival rates, then one would conclude that it was unlikely that photochemical deposition could proceed at a rate

necessary to explain the observed radiator degradation. However, Hayes's background photochemical deposition rate (resulting from chamber residual gas) suggested that a linear extrapolation was inappropriate.

The work discussed in this report extended the measurement of absolute deposition rates into the regime of molecular arrival rates expected on orbit. Figure 20 is a compilation of the laboratory measured deposition rates of model contaminants DC-704 and diethylhexylphthalate [dioctylphthalate (DEHP)], for a variety of substrate conditions, in addition to the results of Hayes. From this figure, one can readily discern the nonlinear dependence of the deposition rate on the molecular arrival rate.

The box in Fig. 20 represents the range of predicted arrival rates and deposition rates necessary to explain the observed increase in solar absorptance of the SDS satellite radiator.[1] The average insolation of the SDS radiator surface has been taken into account in the vertical position of this box. The deposition rates measured in this work fall within the predicted range for a realistic range of substrate temperatures, for two molecules typical of spacecraft outgassing contaminants. Therefore, these data indicate that the unexpected increase in solar absorptance can be ascribed to photochemical contaminant deposition.

B. DEPOSITION MECHANISM

These experiments were done to test the hypothesis that, under the conditions of differing molecular flux and surface temperatures appropriate to actual satellite experience, photochemical deposition is a competition between photolysis and desorption of a transiently adsorbed molecule. This kinetic mechanism for the mass accretion by photochemical deposition can be summarized as

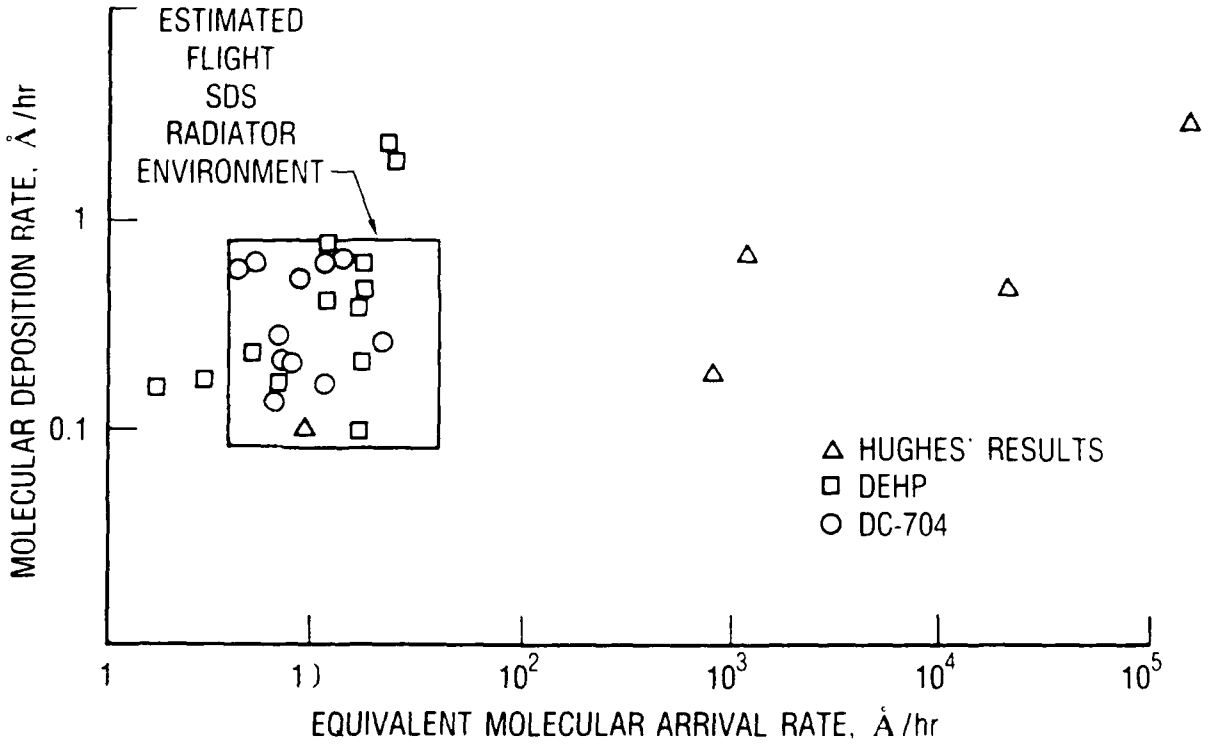

Fig. 20. Compilation of Photochemical Deposition Rates versus Arrival Rate for DC-704 and DEHP for a Variety of Substrate Compositions and Temperatures. Also shown are results from Hughes Aircraft Experiments (see Ref. 1).

$$C + S \underset{k_2}{\overset{k_1}{\rightleftharpoons}} C_s \qquad (2a)$$

$$C_s + h\nu \xrightarrow{k_3} C_s^* \qquad (2b)$$

$$C_s^* \xrightarrow{k_4} B + S \qquad (2c)$$

$$C_s^* \xrightarrow{k_5} C_s \qquad (2d)$$

where C is the potential contaminant molecule, S is a surface site, C_s is a surface-adsorbed contaminant molecule, and B is a photochemically bound contaminant molecule. The nature of excitation to C_s^* is not specified but could include, for example, electronic excitation or radical formation by bond cleavage.

At steady state ($d^2B/dt^2 = 0$), with the assumption of constant total site density ($S + C_s + C_s^* = S_0$), the kinetic model shown in Eqs. (2a)-(2d) predicts an accretion rate of

$$\alpha B/dt \cong \frac{k_3 q I_0 P_0 F_c}{k_2 + k_3 q I_0 + P_0 F_c / S_0} \qquad (3)$$

where $q = k_4/(k_4 + k_5)$. [See Appendix B for the algebraic derivation of Eq. (3).] The results of the photodeposition experiments are consistent with this kinetic model.

The steady-state behavior of this model, assuming constant site density and rate coefficients dependent only on substrate temperature, described very well the isothermal contaminant flux dependence of the

photochemical desposition rate (see Figs. 11 and 12). The cross sections for photoexcitation of the adsorbate, extracted from the data using the kinetic model, are approximately equal to the bulk absorption cross sections of the precursor molecules. The "site densities" inferred from the kinetic data vary by about an order of magnitude, in a range that is reasonable for adsorbate molecules of the size used in this work. When one considers that this variation in site densities is obtained from the coupled slopes and intercepts of two different linearized plots, then such a variation is not unreasonable.

A similar model involving substrate excitation could be proposed. However, an analysis of the data using such a model would require the surface excitation to have an unreasonably long lifetime of hundreds of seconds and a surprisingly small effective VUV absorptivity for the contaminated metal substrate. Furthermore, excitation of the substrate by VUV radiation, resulting in eventual reaction of the contaminant molecule, is not considered a probable mechanism based on the fact that photodeposit was observed on an MgF_2 witness sample. MgF_2 is transparent to 150 to 190 nm radiation, thus precluding any substrate excitation.

The negative apparent activation energy for photodeposition also shows that the deposition rate is dependent upon the surface concentration of the adsorbed molecule. It is difficult to propose any other phenomenon to account for the negative value for the activation energy. This conclusion is supported by the dependence of the photodeposition rate on the substrate composition. This dependence is shown by the lower photodeposition rate on gold versus platinum and by the greater contaminant film thickness on aluminum versus gold.

It is useful to examine the degree to which the kinetic model, shown in Eqs. (2a)-(2d), can describe the substrate temperature dependence of the deposition rate. The available data permit only the simplest implementation of the model, which assumes that only the rate coefficient for desorption, k_2, is temperature dependent and that it exhibits simple Arrhenius behavior, independent of surface coverage.

Figures 21 and 22 show how this temperature-dependent model is used to describe the measured deposition rates for the two different precursor molecules, DEHP and DC-704. (Values for P_0 and k_3q were obtained from the isothermal flux dependence of the deposition rates. The thermal desorption rate coefficient came from the first-order desorption rate measurements.) The model describes the temperature dependence of the DEHP deposition rate much better than that of the DC-704 deposition rate.

A significant difference between the two molecules is that the activation energy for desorption, E_a, of the first adsorbed monolayer of DC-704 was measured to be significantly less than the heat of vaporization, H_v, of the bulk liquid; whereas for DEHP, E_a was slightly greater than H_v. These discrepancies between E_a and H_v guarantee that the assumption of simple Arrhenius behavior of k_2 will be valid only for low flux and/or high substrate temperature, in which the steady-state concentration of adsorbed, virgin contaminant molecules is less than a monolayer.

As the flux is increased, or as the substrate temperature is decreased, the effects of multilayer adsorption (or bulk condensation) become more pronounced. For $E_a < H_v$, the transition to bulk condensation results in a sharp decrease in the desorption rate coefficient (and a concomitant increase in the net deposition rate). For $E_a > H_v$, lowering the temperature or increasing the flux does not produce such a sharp drop in k_2. In other words, if the flux is high enough, or if the temperature is low enough, the surface coverage in the absence of illumination does not approach a steady-state value. Rather, condensation continues, and the temperature or flux at which this change from steady-state to bulk condensation effectively occurs depends on the relative values of E_a and H_v.

Therefore, it is not surprising that the simple implementation of this Langmuir kinetic model is more successful in describing the temperature dependence of photochemical deposition for $E_a > H_v$ than for $E_a < H_v$. Such considerations highlight the fact that to be valid over a wide range of surface temperatures and molecular fluxes, a model of photochemical deposition should account for the effects of multilayer adsorption. However, if

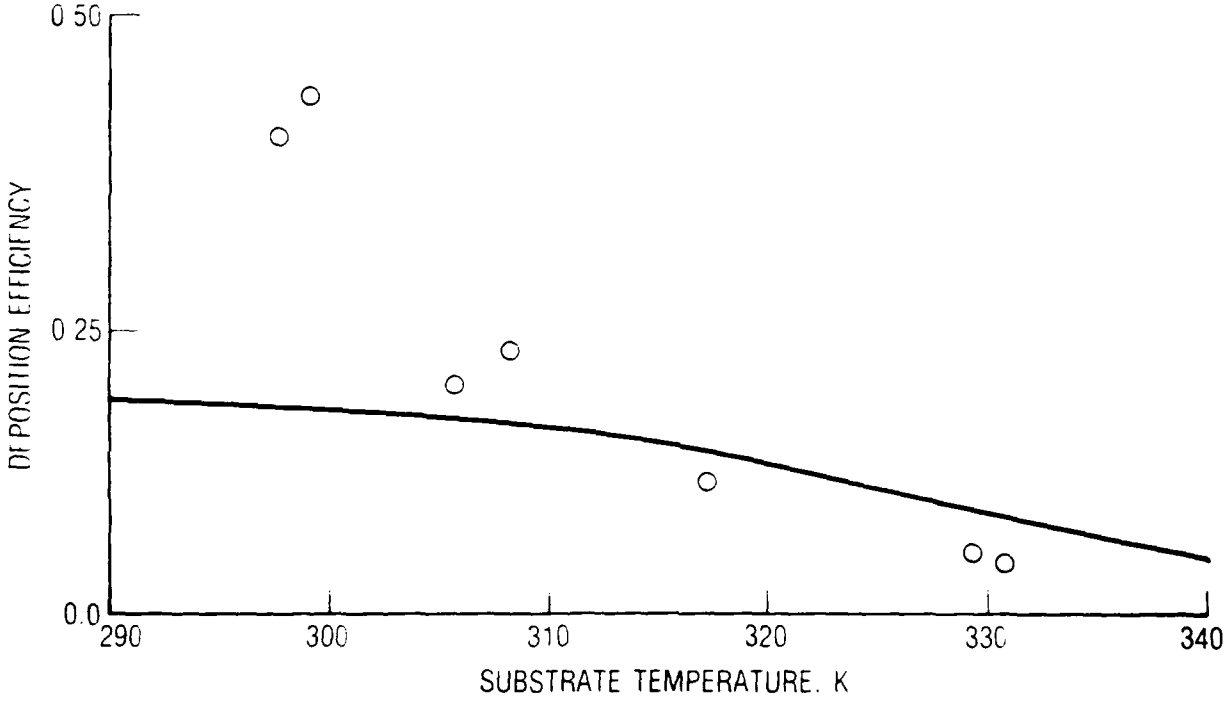

Fig. 21. Temperature Dependence of the Rate of Photochemical Deposition of DC-704 at Constant Incident Flux. The solid line is the prediction of the simple kinetic model assuming only the coefficient of thermal desorption of virgin DC-704 is temperature dependent.

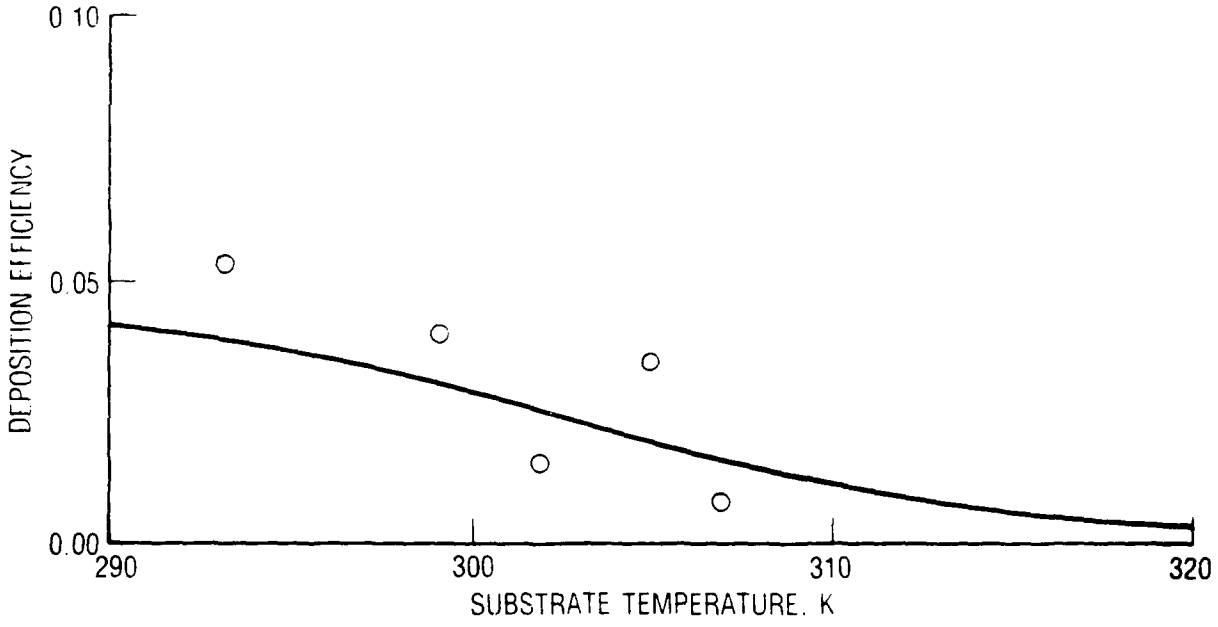

Fig. 22. Temperature Dependence of the Rate of Photochemical Deposition of DEHP at Constant Incident Flux. The solid line is the prediction of the simple kinetic model assuming only the coefficient of thermal desorption of virgin DEHP is temperature dependent.

one accepts the limitations of its several simplifying assumptions, the simple kinetic model can be useful in predicting the magnitude of the problem presented by steady-state photochemical contaminant deposition on spacecraft.

C. COMPARISON TO SCATHA ML-12 RESULTS

The inverse temperature dependence of the measured photochemical deposition rates appears to differ somewhat from the results of the SCATHA ML-12 experiment. No temperature dependence of the rate of mass accumulation on the ML-12 belly band TQCM (ascribed to photochemical deposition) can be discerned from the data[2,3] (see Figs. 2 and 3). The following observations can be made about the difference in experimental results. The ML-12 sensors are subject to a varying flux of contaminant molecules because of the slow depletion of contaminant sources and slow fluctuations in vehicle temperature. In addition, solar illumination is not constant: it varies with time of the year, with the drifting vehicle attitude, and with the once-per-minute rotation of the vehicle. These and other environmental fluctuations result in a "noise" or uncertainty in the short-term mass accretion rate of at least a factor of 2. This uncertainty could mask any possible temperature dependence of the ML-12 photochemical deposition rate.

There is a greater difficulty in comparing our laboratory results to the ML-12 results: the absolute fluxes and identities of potential contaminant molecules on the ML-12 TQCM are completely unknown. Even ignoring the possibility of bulk condensation, the proposed kinetic model for photochemical deposition predicts a low temperature limit for the deposition rate, which is reached when $k_2 << (k_3 q + P_0 F_c / S_0)$. Indeed, this model predicts that for any given values of the desorption energy and flux, there is a relatively wide range over which the deposition is temperature insensitive. The temperature and rapidity at which this limit is reached vary strongly with the desorption energy (identity) of the contaminant molecule and its arrival rate. The "Langmuir" type model predicts that the limiting low temperature increases monotonically with the desorption energy

(at constant flux) and that the onset of the low temperature limit becomes shallower with decreasing flux (at constant desorption energy).

The experiments described in this report used contaminant flux ranges that were selected on the basis of the relatively high predicted molecular arrival rates for the SDS radiator surface. The temperature ranges were chosen so that bulk condensation would not occur. This second criterion automatically selects temperatures that are above or near the low temperature limit. Thus, for photodeposition of a single molecule, one would expect to observe a substrate temperature effect that could be well characterized by a single desorption energy. There is no such predisposition in the ML-12 experiment. Therefore, the perceived discrepancy between the laboratory results and ML-12 results does not necessarily imply that photochemical deposition is not the dominant process accounting for the mass accretion observed on ML-12. The discrepancy does suggest that the thermochemistry and arrival rates differ substantially between the ML-12 and the laboratory experiments.

In summary, absolute rates for VUV deposition of organic contaminant films have been measured. The contaminant deposition rates are large enough to explain the unexpectedly high rate of degradation of the SDS radiator. A simple kinetic model using experimentally measured parameters is reasonably successful in describing the process. These results and data from the SCATHA ML-12[3] spaceflight experiment show quantitatively that solar UV irradiation does not merely darken or fix previously condensed contaminant films; it also significantly affects the rate at which those films accrete. Therefore, VUV photodeposition is a viable contamination mechanism that should be considered whenever spacecraft contamination predictions or budgets are made.

REFERENCES

1. D. F. Hall, T. B. Stewart, and R. R. Hayes, "Photo-Enhanced Spacecraft Contamination Deposition," AIAA 20th Thermophysics Conference, Paper No. 85-0953, Williamsburg, VA, 19-21 June 1985.

2. D. F. Hall, "Flight Experiments to Measure Contamination Enhancement by Spacecraft Charging," Proc. Soc. Photo-Opt. Inst. Eng. Vol. 216, pp. 131-138 (paper presented in Los Angeles, CA, 4 February 1980).

3. D. F. Hall, "Current Flight Results from the P78-2 (SCATHA) Spacecraft, Contamination and Coating Degradation Experiments," Proc. Int. Symp. on Spacecraft Materials in Space Environment, p. 143 (paper presented in Toulouse, France, 8 June 1982).

4. R. Kruger and H. Shapiro, "Experiments on the Effect of Ultraviolet on Contamination in Vacuum Systems," TM 81999, NASA, Washington, D.C. (August 1980).

5. P. D. Fleischauer and L. U. Tolentino, "The Far Ultraviolet Photolysis of Polymethylphenylsiloxane Films on Quartz Substrates," Proceedings of the Seventh Conference on Space Simulation, NASA-SP-336 (1973), p. 645 (paper presented in Los Angeles, CA, 12-14 November 1973).

6. R. W. Phillips, L. U. Tolentino, and S. Feuerstein, "Spacecraft Contamination under Simulated Orbital Environment," J. Space and Rockets 14(8), 501 (1977).

7. J. Y. Tsao and D. J. Ehrlich, "UV Laser Photopolymerization of Volatile Surface-Adsorbed Methylmethacrylate," Appl. Phys. Lett. 42(12), 997 (1983).

8. D. H. Maylotte and A. N. Wright, "Surface Polymerization of Tetrafluoroethylene," Faraday Discuss. Chem. Soc. 58, 292 (1975).

9. A. W. Adamson, Physical Chemistry of Surfaces, Wiley, New York (1982).

10. P. A. Small, K. W. Small, and P. Cowley, "The Vapor Pressure of Some High Boiling Esters," Trans. Farady Soc. 44, 810 (1948).

11. Dow Corning, Diffusion Pump Fluids, Bulletin 05-058 (September 1963).

12. B. L. Sowers, M. W. Williams, R. N. Hamm, and E. T. Arakuwa, "Optical Properties of Some Silicone Diffusion Pump Oils in Vacuum Ultraviolet Using a Closed-Cell Technique," J. Appl. Phys. 42(11), 4252 (1971).

13. R. J. Partridge, "Vacuum-Ultraviolet Absorption Spectrum of Polystyrene," J. Chem. Phys. 47(10), 4223 (1967).

14. C. D. Wagner, W. M. Riggs, L. E. Davis, and J. F. Moulder, Handbook of X-ray Photoelectron Spectroscopy, ed., G. F. Muilenberg, Perkin-Elmer, Physical Electronic Div. (1979).

15. S. Siegel and T. B. Stewart, "Vacuum-Ultraviolet Photolysis of Polydimethylsiloxane, Gas Yields and Energy Transfer," J. Phys. Chem. 73, 823 (1969).

APPENDIX A
APPARATUS

All experiments were performed in an ultrahigh vacuum system evacuated with a combination of a turbomolecular pump and a liquid nitrogen cooled (110 K) shroud to pressures of about 2×10^{-9} Torr. Thus, possible interference from background contaminants in the chamber was greatly reduced. The experimental chamber configuration, illustrated in Fig. A-1, consists of a temperature-controlled quartz crystal microbalance (TQCM) for mass detection, a Knudsen cell, or effusive molecular beam source of model contaminant molecules, interchangeable vacuum ultraviolet (VUV) lamps for the radiation source, and a shutter for switching the molecular beam on and off to the TQCM.

A. TQCM

The keystone of this experiment was the measurement, by the TQCM, of mass deposited on the surface in minute amounts (10^{-8} g cm^{-2}). A doublet crystal was used with two electrode pairs (a reference pair and a sample pair) plated onto a single quartz crystal to maintain both electrodes in an identical thermal environment. The reference pair was shielded with a sapphire window.

The frequency of oscillation of each electrode pair was nominally either 5 or 10 MHz, depending on the crystal thickness used. The difference in frequency between the two electrode pairs generated a beat frequency, which was obtained by mixing the outputs of the oscillators that drove the crystals. The frequency of the sample electrode was lowered by the addition of mass to the surface. The resulting change in beat frequency was directly proportional to the mass accumulated on the sample electrode. The mass sensitivities of the 5 and 10 MHz crystals were 1.77×10^{-8} g cm^{-2} Hz^{-1} and 4.42×10^{-9} g cm^{-2} Hz^{-1}, respectively.

The TQCM electrodes were made from platinum, aluminum, or gold and were the primary substrate used for photodeposition. The sapphire window

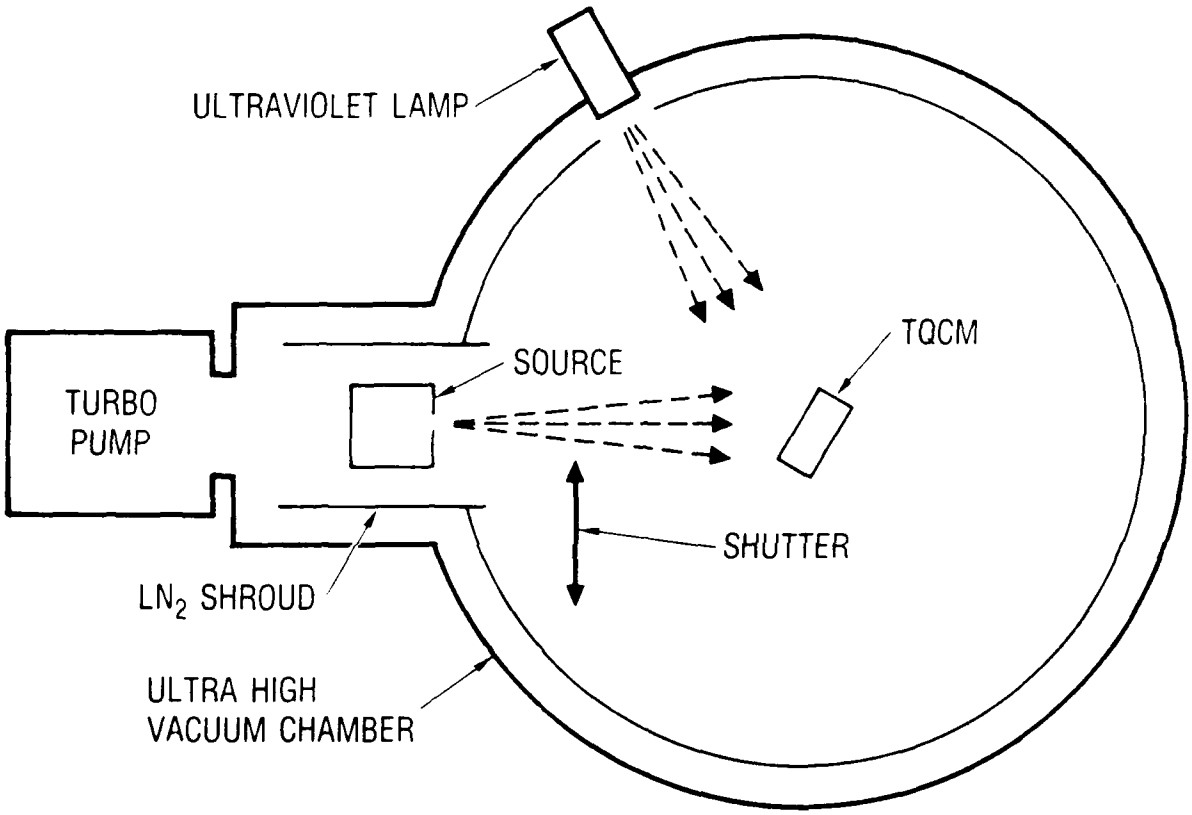

Fig. A-1. Schematic Representation of the Photochemical Deposition Apparatus

shielded the reference pair of electrodes from the molecular flux but permitted irradiation by VUV photons. This was done to minimize possible thermal effects caused by uneven heating of the crystal electrodes by the VUV radiation.

The TQCM was mounted on a large temperature-controlled copper block, which prevented large temperature fluctuations during mass deposition. The block temperature was controlled to ± 0.5 K by a time proportional temperature controller. The fluctuations in the TQCM temperature limited the ultimate sensitivity of the TQCM. The thermal fluctuations were of two types: (1) short-term changes over about 1 to 2 min or less and (2) long-term cyclic changes over approximately 6 h. The maximum temperature excursions were 1 K for both types of fluctuations. For the 10 MHz crystal, the temperature changes appear as an effective mass change of 0.9 to 4.4×10^{-8} g/cm^{-2}. Signal averaging over 10 min was used to compensate for the short-term fluctuations. A linear temperature correction was used to compensate for long-term fluctuations, using the following expression

$$F - F_o + Z\,(T - T_o) \qquad (A\text{-}1)$$

where F_o is the reference frequency for a given experiment at temperature T_o, T is the actual time-dependent temperature, and Z is an empirically determined frequency-temperature correction factor. This thermal coefficient for the 5 and 10 MHz crystals ranged from -2.0 to 10 Hz/K.

The lower limit of the estimated rate of deposition on the SDS satellite was about 10^{-9} g cm^{-2} h^{-1}, which is within this temperature-induced noise level. To measure the low deposition rates with certainty, the crystal frequency was averaged over some fixed time period, typically 5 to 10 min, to reduce the effect of short-term thermal fluctuations. The deposition was continued until a net mass change occurred equal to twice that attributed to thermal fluctuations. These averaging operations, together with application of the empirically determined temperature-frequency correction, permitted the measurement of deposition rates to as low as 10^{-9} g cm^{-2} h^{-1}.

The TQCM was positioned in the vacuum chamber and oriented to permit the molecular beam and the photon beam to impinge on the surface at angles of incidence of -30 and +30 deg with respect to the surface normal. The incident beams intersected each other at the TQCM sample electrode surface.

B. KNUDSEN CELL

The molecular beam was produced by the effusion of the model contaminant molecule from a Knudsen cell. The cell was constructed from a 1-in.-diam copper cylinder. The cylinder had an end plate with an 80-mils-diam hole through which the molecules would effuse. For these experiments, two molecules, DC-704 (siloxane) (tetramethyltetraphenyltrisiloxane) and DEHP [bis (2-ethylhexyl)phthalate], were used as model contaminants. These molecules were selected because they were representative of two major classes of compounds found in spacecraft components and on spacecraft surfaces.[A-1] The structure and associated bond strengths are given in Figs. A-2 and A-3. These compounds have very well-defined vapor pressure-temperature relationships, so the arrival rate of the molecules to the TQCM could be readily controlled by adjusting the cell temperature.

The impingement rate F_c was determined by cooling the TQCM to 90 K and measuring the rate of mass increase as a function of Knudsen cell temperature with the shutter opened. The rate of mass increase is equal to the impingement rate, if the sticking coefficient for these molecules is unity, which is likely to be a good approximation because of the very small vapor pressures of these materials at 90 K. By plotting the change in crystal frequency as a function of time and using the crystal frequency mass relation, the impingement rate can be determined.

A series of measurements was made at various Knudsen cell temperatures. Through an extended form of the Clausius-Clapeyron relation ($F_c = A\exp[\Delta H_v/RT]$), one can determine the molecular arrival rate for any Knudsen cell temperature. The actual Clausius-Clapeyron relation equates the vapor pressure of a fluid to its temperature. We have made the simplifying assumption that the temperature dependence of F_c is contingent only on the variation of the source material's vapor pressure. If this assumption is

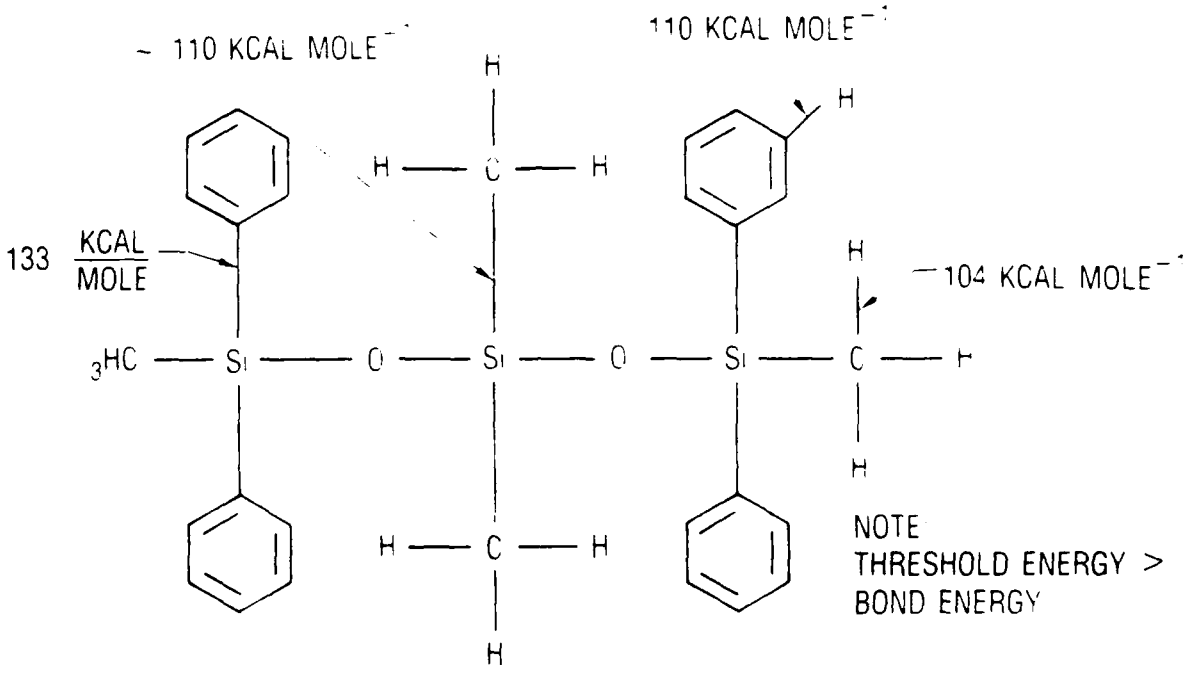

Fig. A-2. Structure of DC-704 (Tetramethyltetraphenyltrisiloxane), with Approximate Bond Strengths Indicated

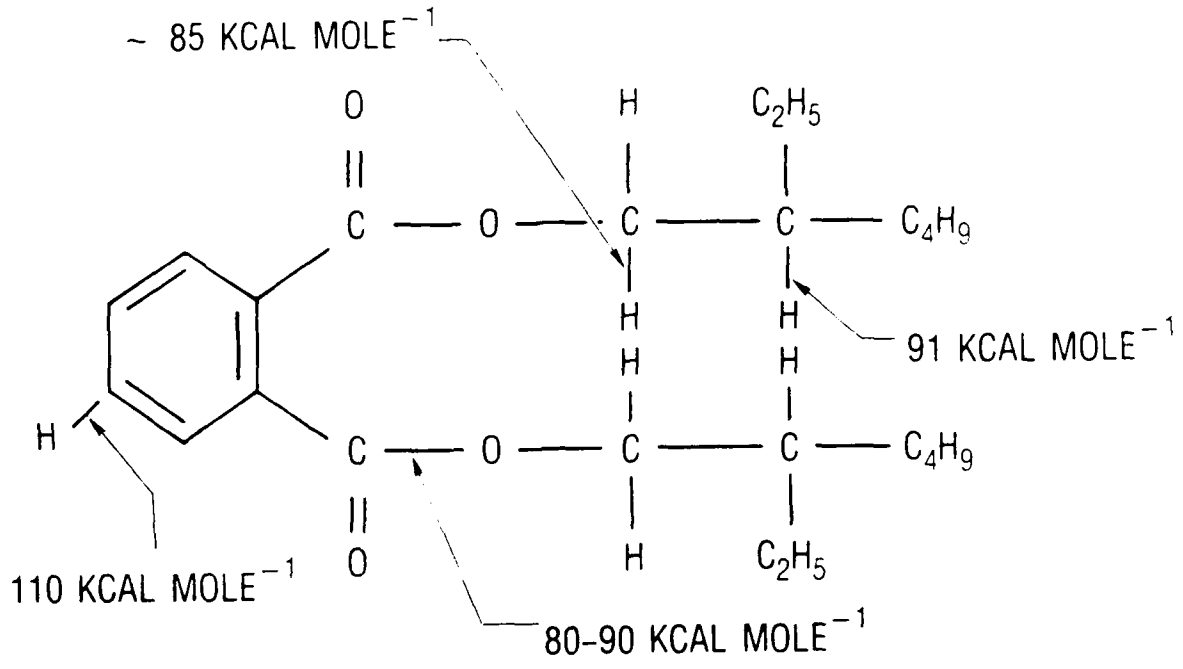

Fig. A-3. Structure of DEHP [Bis (2-ethylHexyl)phthalate], with Approximate Bond strengths Indicated

correct, then a plot of ln F_c versus 1/T should give a straight line with a slope of ΔH_v and an intercept of ln A. The results for DC-704 and DEHP are shown in Figs. A-4 and A-5, respectively. The values obtained for the heat of vaporization of DC-704 and DEHP are H_v = 23.8 and 27.5 kcal $mole^{-1}$, respectively. These values are quite close to the published values for the heat of vaporization of these molecules,[A-2,A-3] which, together with the good fits, support the Clausius-Clapeyron assumption.

The computed arrival rates for DC-704 and DEHP at any given temperature are given by Eqs. (A-1) and (A-2), respectively:

$$F_c(\text{DC-704}) = 1.11 \times 10^5 \text{ g cm}^{-2} \text{ sec}^{-1} \exp(-23.8 \text{ kcal mole}^{-1}/RT) \quad \text{(A-2)}$$

$$F_c(\text{DEHP}) = 1.92 \times 10^8 \text{ g cm}^{-2} \text{ sec}^{-1} \exp(-27.6 \text{ kcal mole}^{-1}/RT) \quad \text{(A-3)}$$

These empirically determined molecular fluxes are in excellent agreement with those predicted from simple kinetic theory and the apparatus geometry, which justifies the approximations made in this calibration.

C. RADIATION SOURCE

The radiation sources for these experiments were rare gas resonance lamps with a spectral output of intensity similar to the solar spectrum for a particular wavelength range. The lamps were excited in a quarter-wave-foreshortened coaxial microwave cavity with power coupling and tuning of the Evenson design.[A-4] A 2450 MHz magnetron supplied power to the cavity. These lamps were filled with krypton or xenon to a pressure of approximately 300 Torr. The moderate pressure broadens the spectral output, producing a continuum emission over the particular energy range. The emission spectra of the lamps are shown in Fig. A-6.[A-5]

The lamps were attached to the vacuum system by ultrahigh vacuum flanges with the windows extending into the vacuum system. The lamp fluxes at the sample, calibrated by carbon dioxide actinometry,[A-6] were measured to be 4.9×10^{12} and 6.9×10^{12} photons cm^{-2} sec^{-1} for the krypton and

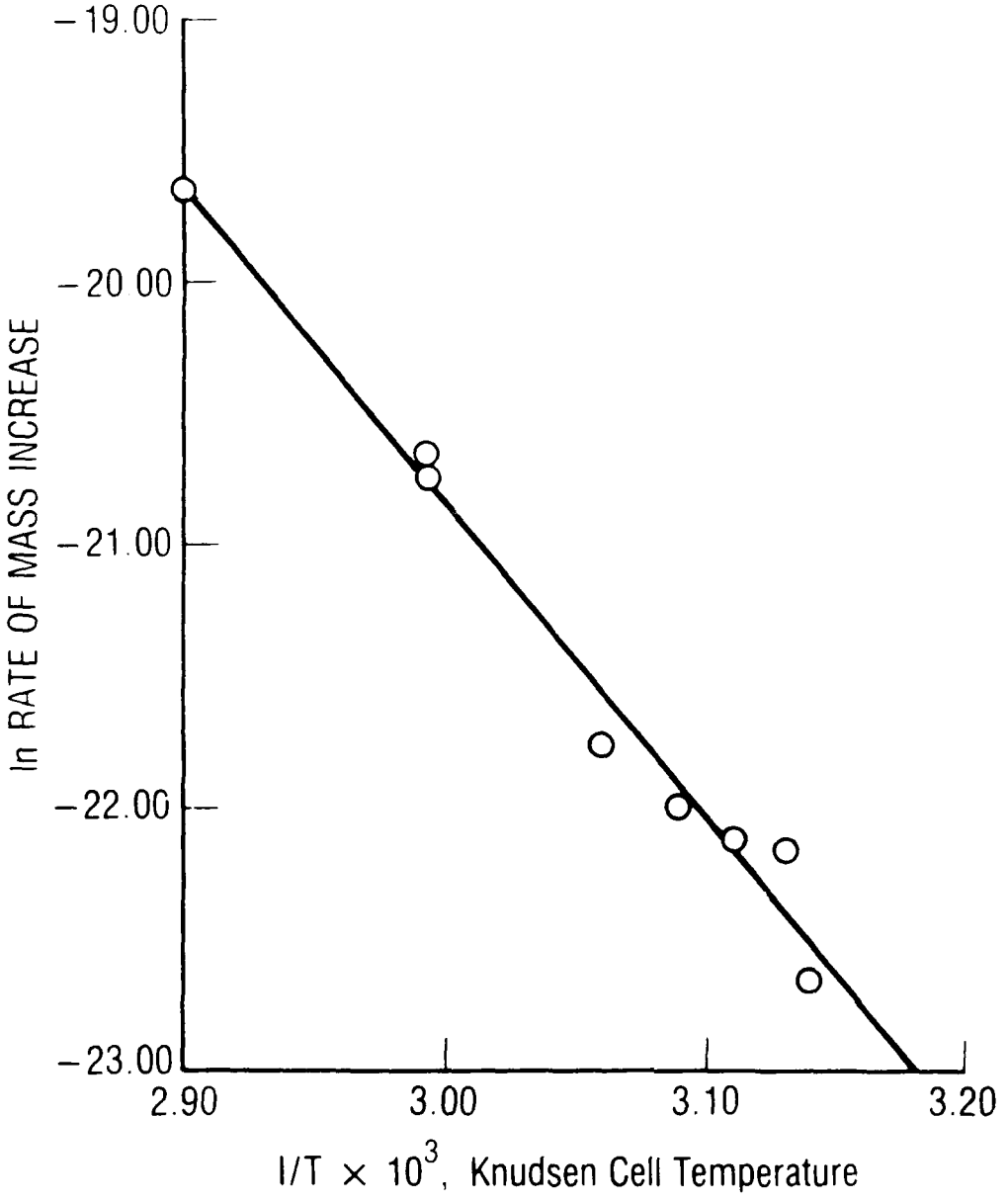

Fig. A-4. Arrhenius Plot (in Source Temperature) of the Deposition Rate of DC-704 on a 90 K Quartz Crystal Microbalance. The solid line is a linear least-squares fit.

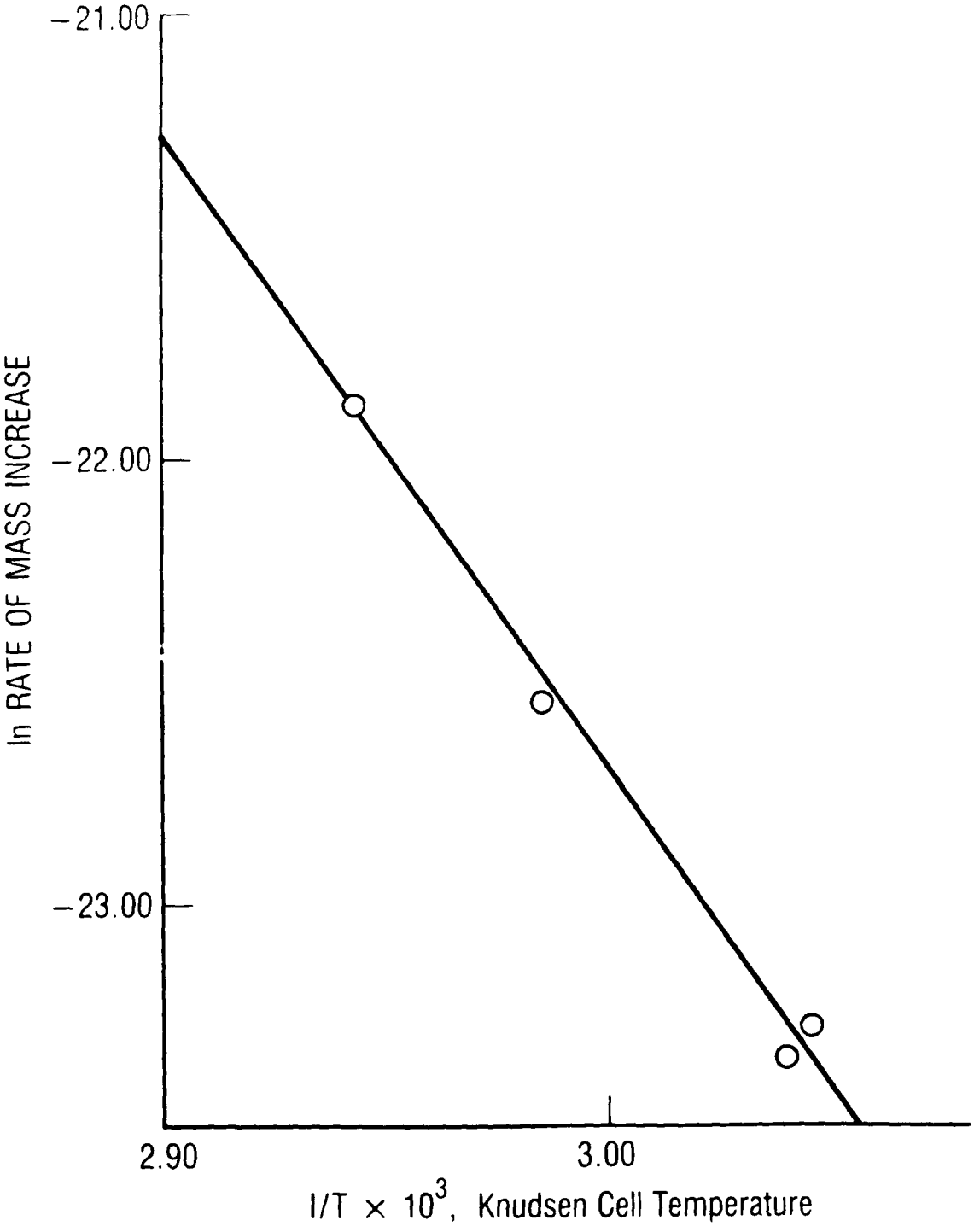

Fig. A-5. Arrhenius Plot (in Source Temperature) of the Deposition Rate of DEHP on a 90 K Quartz Crystal Microbalance. The solid line is a linear least-squares fit.

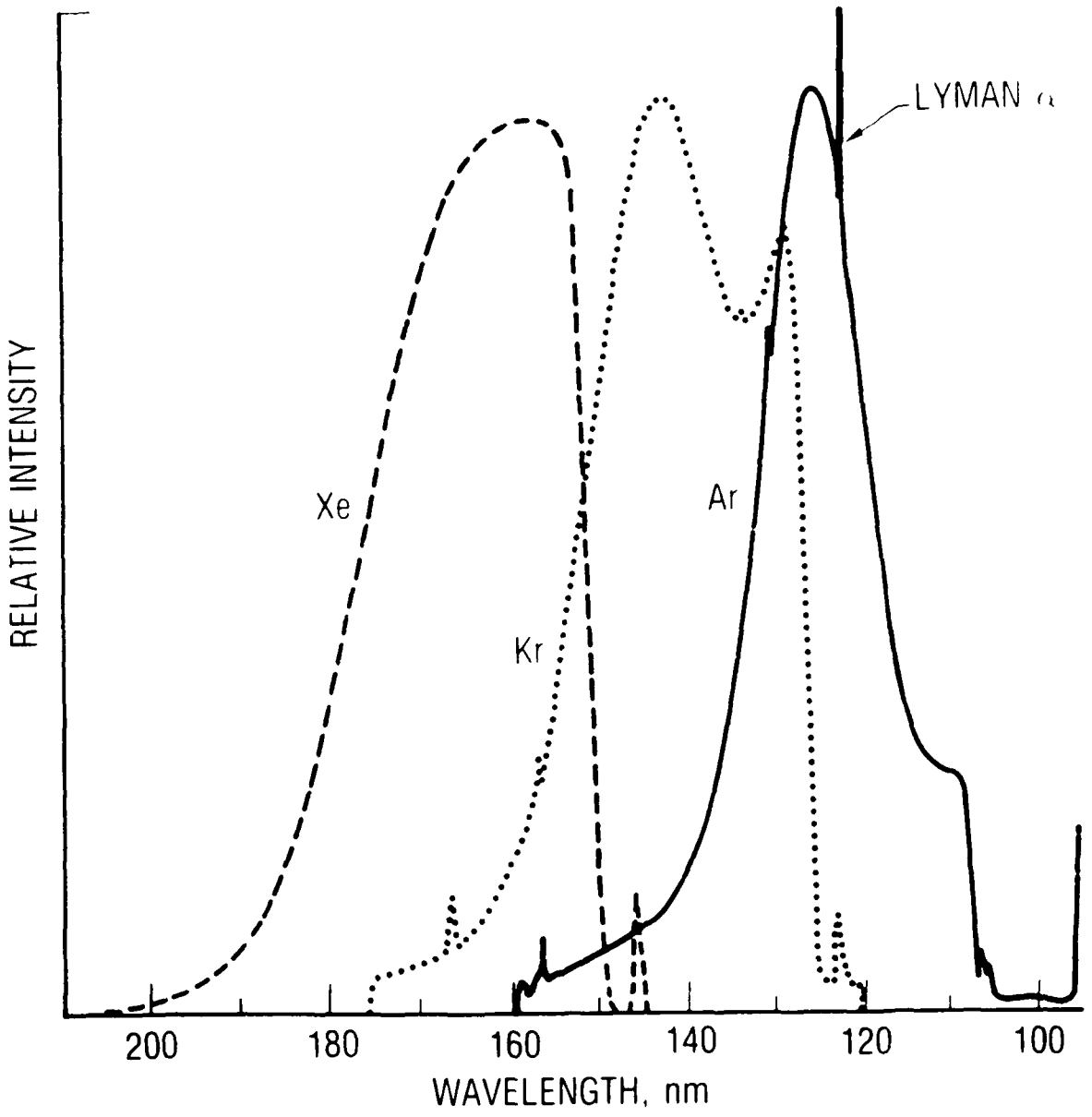

Fig. A-6. Emission Spectra of Xe, Kr, and Ar Microwave-Excited Resonance Lamps (after Ref. 5)

xenon lamps, respectively. These values compare quite closely to the integrated solar intensity of 9×10^{12} photons cm^{-2} sec^{-1} in the 130-190 nm range or 2.3×10^{12} photons cm^{-2} sec^{-1} in the 130-180 nm region.[A-7]

D. WITNESS SAMPLES

Witness samples were placed around the TQCM to measure the effect of substrate surface composition on the contaminant deposition rate. If the deposition resulted from adsorption of the contaminant onto the surface before photolysis, then the difference in surface composition might have an effect on the adsorption rate and consequently on the overall photodeposition rate. In addition, witness samples with different VUV absorption cross sections were used to test for possible substrate involvement in the photolysis process.

Witness samples were made of polished aluminum disks 1/4 in. in diameter, either bare or coated with 1000 Å of gold or MgF_2. Some samples were masked during coating so that half of their surface was gold or MgF_2 and the other half was aluminum. Such configurations were selected to minimize any possible variations in deposition rates resulting from mounting position of the witness samples. These samples were exposed to the contaminant molecules in the absence and presence of radiation and were then analyzed by X-ray photoelectron spectroscopy and Auger electron spectroscopy.

REFERENCES

A-1. J. A. Colony, "Ultraviolet Absorption of Common Spacecraft Contaminants," TM 80551, NASA, Washington, D.C. (August 1979).

A-2. Dow Corning, Diffusion Pump Fluids, Bulletin 05-058 (September 1963).

A-3. P. A. Small, K. W. Small, and P. Cowley, "The Vapor Pressure of Some High Boiling Esters," Trans. Farady Soc. 44, 810 (1948).

A-4. F. C. Fehsenfeld, K. M. Evenson, and H. P. Broida, "Microwave Discharge Cavities Operating at 2450 MHz," Review of Scientific Instruments 36, 294-298 (March 1965).

A-5. J. R. McNesby, W. Brown, and J. Ball, "Vacuum-Ultraviolet Techniques in Photochemistry," in Creation and Detection of the Excited States, ed., A. A. Lamola, Dekker (1976).

A-6. T. G. Slanger and G. Black, "The CO_2 Photolysis Problem," J. Chem. Phys. 54(3), 1889 (1971).

A-7. Solar Constant and Air Mass Zero Solar Spectral Irradiance Tables, ASTM Standard E 490-73a, p. 436.

APPENDIX B

KINETIC MODEL OF PHOTOCHEMICAL FILM DEPOSITION

A kinetic model for the photodeposition process, based on a competition between photolysis and desorption of a transiently adsorbed molecule, was used as a guide for experimentation and as a tool for analyzing the results. The first section of this appendix presents the kinetic mechanism for the mass accretion of contaminants by photodeposition. The section also presents an algebraic development of the steady-state behavior predicted by the mechanism with the assumption of constant adsorption site density and rate coefficients independent of coverage.

A. PHOTOCHEMICAL DEPOSITION MECHANISM

A simple mechanism for the mass accretion of contaminants by photochemical deposition can be summarized as

$$C + S \underset{k_2}{\overset{k_1}{\rightleftharpoons}} C_s \qquad \text{(B-1a)}$$

$$C_s + h\nu \xrightarrow{k_3} C_s^* \qquad \text{(B-1b)}$$

$$C_s^* \xrightarrow{k_4} B + S \qquad \text{(B-1c)}$$

$$C_s^* \xrightarrow{k_5} C_s \qquad \text{(B-1d)}$$

where C is the potential contaminant molecule, S is a surface site, C_s is a surface-adsorbed contaminant molecule, and B is a photochemically bound contaminant molecule. The nature of excitation to C^* is not specified but

could include, for example, electronic excitation or radical formation by bond cleavage.

At steady state ($d^2B/dt^2 = 0$), with the assumption of constant total site density ($S + C_s + C_s^* = S_0$), this kinetic model predicts an accretion rate of

$$dB/dt = \frac{k_1 k_3 q I_0 C S_0}{k_2 + k_3 q I_0 + k_1 C(1 + q k_3 I_0 / k_4)} \qquad \text{(B-2)}$$

where q, the "quantum yield," is $k_4/(k_4 + k_5)$ and I_0 is the light flux. The quantity qk_3I_0/k_4 in Eq. (B-2) is, in fact, the ratio of the steady-state population of C_s^* to that of C_s. It is assumed that this ratio is substantially less then 1. Thus

$$dB/dt \cong \frac{k_1 k_3 q I_0 C S_0}{k_2 + k_3 q I_0 + k_1 C} \qquad \text{(B-3)}$$

All quantities in Eq. (B-3) have dimensions, except for q. The surface concentrations have units of particles per unit area. I_0 has units of photons per unit area per unit time. The rate coefficients k_2, k_4, and k_5 have units of frequency (reciprocal time). The rate coefficient k_3 has units of area.

The quantity k_1C is readily understood by considering that, at time zero, when the surface is clean, the rate of accretion of adsorbed contaminant is given by

$$dC_s/dt = k_1 C S_0 = P_0 F_c \qquad \text{(B-4)}$$

where F_c is the incident flux of potential contaminant molecules (in particles per unit area per unit time) and P_0 is the probability that a molecule striking an unoccupied surface site will stick to the site. For

this model, it is assumed that this "sticking coefficient" is independent of the surface coverage; therefore, one can make the substitution $k_1 C = P_0 F_c / S_0$, which yields

$$dB/dt \cong \frac{k_3 q I_0 P_0 F_c}{k_2 + k_3 q I_0 + P_0 F_c / S_0} \qquad \text{(B-5)}$$

If one defines the reaction efficiency, e, to be $(dB/dt)/F_c$, then a plot of the reciprocal of the reaction efficiency versus F_c should be a straight line

$$e^{-1} = \frac{k_2 + k_3 q I_0}{k_3 q I_0 P_0} + \frac{F_c}{k_3 q I_0 S_0} \qquad \text{(B-6)}$$

B. STEADY-STATE ADSORPTION ISOTHERM

The steady-state behavior of the proposed mechanism in the absence of illumination is analogous to the Langmuir adsorption isotherm of a gas adsorbed onto surfaces under equilibrium conditions. The steady-state solution of Eq. (B-1a) yields

$$F_c = \frac{F_c S_0}{C_s} = \frac{k_2 S_0}{P_0} \qquad \text{(B-7)}$$

Therefore, a measurement of the steady-state mass accumulation (in the dark, with constant molecular flux) will provide a measure of the surface site density and desorption rate coefficient.